Whip restraint

for a steam pipe rupture event on a

nuclear power plant

Alfred C Pieters

Student Number 23541709

Dissertation submitted in fullfilment of the requirements for the degree
***Master of Engineering* in Mechanical Engineering**
at the Potchefstroom campus of the North-West University

Supervisor: Professor Leon Liebenberg, Pr. Eng.

February 2013

ABSTRACT

One of the requirements of a safe nuclear power plant design is the postulation of the dynamic effects of a steam pipe rupture. The dynamic effects are the discharging fluid and pipe whip on structures, systems or components. A pipe rupture can be caused in the steam pipe system where a defect such as a crack exists.

Multiple factors contribute to the initiation of pipe cracks during the plant's life. Cracks may start microscopically small and over time, with the assistance of cyclic operation, fatigue may elongate the crack. When a steam pipe is cooled by water during an accident, steam condensate may accumulate and form slugs of water. This water will have an effect on the system termed condensation induced water hammer. The cause of the pipe rupture is not addressed in this dissertation.

Pipe rupture can be considered to be either a circumferential or longitudinal break. For the purpose of this dissertation only a circumferential break will be considered.

This research is based on the development of a pipe whip restraint structure to protect the plant environment during a steam pipe rupture event in a nuclear power plant. It focuses on a structural component required to restrain the dynamic energy to an acceptable level.

Whip restraints used in the nuclear industry are typically honeycomb, U-bar and crush pipe types. In this dissertation only the U-bar and crush pipe whip restraints will be considered.

The plant environment, with regards to pipe layout, plays a large role in determining the type of restraint to be used, whether it is U-bar or crush pipe. A whip towards the wall/structure will favor a crush pipe; a whip away from the wall/structure will favor a U-bar restraint. In this project the crush pipe is selected where the whip is towards a wall/structure. The crush pipe also represents a simpler design.

First-order analysis is performed using the energy method to determine the conceptual geometry of the whipping component and the restraint geometry. Second-order analysis includes finite element analysis to verify the first-order results. In this dissertation the concept validation is done using LS-PrePost® for the pre- and post-processing while the analysis is performed using LS-DYNA®. During the second-order analysis it was demonstrated that the energy is successfully absorbed by the crush pipe and thus the first-order analysis is considered adequate.

Key words: pipe rupture, pipe whip, dynamic energy, energy method.

ACKNOWLEDGEMENTS

I wish to thank my supervisor Professor Leon Liebenberg for the continuous encouragement, advice and guidance during the period of this study.

I am also grateful to my fellow engineers for their help and support; especially to Herman Bakker and Kerry McCormack.

Hereby, I wish to express my gratitude to Westinghouse Electric South Africa, especially Danie van der Merwe and Pieter Visser, who assisted with the legality, confidentiality and registration of this subject.

Thank you to Doctor Ken Craig and Doctor Francois du Plooy for the assistance I received during the validation and final stage of this project.

Finally, I would like to thank my wife Lynette and my children, Corné and Barend, for their patience and encouragement, and for the sacrifice that they have made while I completed this dissertation.

TABLE OF CONTENTS

List of figures

List of tables

List of symbols

A_a	Jet area at the asymptotic plane	(m^2)	(ANS, 1998)
A_e	Break plane area	(m^2)	(ANS, 1998)
A_R	Asymptotic area ratio	(dimensionless)	(ANS, 1998)
A_{ZOI}	Zone of influence area	(m^2)	
C_T	Steady-state thrust coefficient	(dimensionless)	(ANS, 1998)
D_a	Jet diameter at the asymptotic plane	(m)	(ANS, 1998)
D_b	Diameter of bumper	(m)	
d_{bar}	Diameter of bar	(m)	
D_c	Jet core diameter	(m)	(ANS, 1998)
D_e	Pipe inside diameter	(m)	(ANS, 1998)
D_p	Diameter of process pipe	(m)	
d_t	Elongation of pipe	(m)	
D_{ZOI}	Zone of influence diameter	(m)	
F_c	Crush load	(kN)	
F_{ci}	Force of crush indenter	(kN)	
F_{cr}	Force of crush pipe	(kN)	
F_e	Equivalent thrust force	(kN)	
F_t	Stiffness force	(kN)	
F_T	Transmitted force	(kN)	
G	Gap between pipe and pipe whip restraint	(m)	
g_m	Gap between crush pipe and process pipe	(m)	
k_1	Elastic ring stiffness	(kN/m)	
k_2	Plastic ring stiffness	(kN/m)	
L	Distance from break plane to target	(m)	(ANS, 1998)
L_1	Distance from plastic hinge to pipe whip restraint	(m)	
L_2	Length of plastic hinge	(m)	
L_3	From hinge point to static plastic hinge	(m)	
L_4	From elbow to static plastic hinge	(m)	
L_a	Distance from break plane to asymptotic plane	(m)	(ANS, 1998)
L_c	Core length	(m)	(ANS, 1998)
L_{cp}	Length of crush pipe	(m)	
L_{DH}	Length of dynamic hinge	(m)	
L_{hinge}	Length to hinge point	(m)	
L_s	Static plastic hinge length	(m)	

L_{ZOI}	Zone of influence length	(m)	
M_{el}	Total point mass	(kg)	(Roemer and East, 1980)
m_p	Point mass of pipe	(kg)	
M_p	Plastic moment	(kN.m)	
M_s	Steady-state moment	(kN.m)	(Roemer and East, 1980)
n	Number of bars	(dimensionless)	
P_o	Initial pressure in the source	(kPa)	(ANS, 1998)
r_b	Radius of bumper	(m)	
r_p	Radius of process pipe	(m)	
T	Higher magnitude force	(kN)	
t_{cp}	Minimum thickness of crush pipe	(m)	(Spada and Goldstein, 1980)
T_{INT}	Initial thrust force	(kN)	(ANS, 1998)
T_{jet}	Jet thrust force	(kN)	
t_p	Wall thickness of process pipe	(m)	(Spada and Goldstein, 1980)
T_{pipe}	Pipe thrust force	(kN)	
t_{ss}	Time to reach steady-state thrust force	(seconds)	
T_{SS}	Steady-state thrust force	(kN)	(ANS, 1998)
T_x	Fluid thrust	(kN)	(ANS, 1998)
U	Potential energy	(kJ)	
U_m	Strain energy	(kJ)	
x	Distance from elbow to pipe whip restraint	(m)	
ΔT_{sub}	Jet sub-cooling at stagnation condition	(K)	(ANS, 1998)
δ	Deflection of pipe wall	(m)	
δ_c	Collapse deformation of crush pipe	(m)	
δ_M	Maximum collapse deformation of crush pipe	(m)	

List of abbreviations

ANS	American Nuclear Society
ANSI	American National Standards Institute
ASME	American Society of Mechanical Engineers
CFR	Code of Federal Regulations
CP	Crush pipe
EPRI	Electric Power Research Institute
FEA	Finite element analysis
GDC	General design criterion
HE	High energy
LBB	Leak-before-break
LOCA	Loss-of-coolant accident
LSTC	Livermore Software Technology Corporation
ME	Moderate energy
OLP	Overlay plate
n.a.	Not applicable
NB	Nominal bore
NPP	Nuclear power plant
NRC	Nuclear Regulatory Commission
NUREG	Nuclear regulation
OLP	Overlay plate
PVP	Pressure vessels and piping
PWR	Pipe whip restraint
RZOI	Restrained zone of influence
SSC	Structures, systems or components
USNRC	United States Nuclear Regulatory Commission
UZOI	Unrestrained zone of influence
WR	Whip restraint

Nomenclature

Break

A sudden, gross failure of the pressure boundary of a pipe; either in the form of a complete circumferential severance (guillotine break) - labeled circumferential break - or a sudden longitudinal split - labeled longitudinal break.

Condensation induced water hammer

A rapid condensation event or a rapid steam bubble collapse event. It occurs when a steam pocket becomes totally entrapped in sub-cooled condensate. As the trapped steam gives up its heat to the surrounding condensate and pipe walls, the steam changes from a vapour state to a liquid state. As a liquid, the volume formerly occupied by the steam shrinks by a factor ranging from several hundred to over a thousand, depending on the saturated steam pressure. Likewise, the pressure in the void drops to the saturated vapour pressure of the surrounding condensate (for example, the saturated vapour pressure of condensate at ambient temperature is less than 7 kPa atmospheric). This leaves a low pressure void in the space formally occupied by the steam. The surrounding condensate still under steam pressure will rush in to fill the void. The resulting collision of condensate generates an over-pressurization that reverberates throughout the section of pipeline filled with condensate. Since condensate is virtually incompressible; in a collision it does not give.

Class 1 piping

Piping designed to the American Society of Mechanical Engineers (ASME) Boiler and Pressure Vessel Code, section III (ASME, 2004b).

Dynamic hinge

The location of plastic deformation due to pure bending and dynamic loading where inertial effects are considered.

Fluid decompression transient

The pressure transient and corresponding load transient that occurs inside a piping system as a result of a postulated pipe break. This includes pump overspeed effects as a result of postulated pipe break.

High-energy (HE) lines

Systems, or portions of systems, in which the maximum normal operating temperature exceeds 93.3°C or the maximum normal operating pressure exceeds 1896 kPa (gauge pressure) with the exception of lines that exceed 93.3°C or 1896 kPa (gauge pressure) for 2% or less of the time that the system is in operation; or for less than 1% of the plant operation time, which are considered moderate energy.

Indication

The response or evidence from an examination such as a blip on the screen of an instrument. Indications are classified as true or false. False indications are those caused by factors not related to the principles of the testing method or by improper implementation of the method, such as film damage in radiography or electrical interference in ultrasonic testing. True indications are further classified as relevant and non-relevant. Relevant indications are those caused by flaws. Non-relevant indications are those caused by known features of the tested object, such as gaps, threads or case hardening.

Leakage crack

Shall be assumed to be a crack through the pipe wall where the size of the crack and corresponding flow rate are determined by analysis and a leak detection system (ANS, 1998).

Moderate-energy (ME) lines

Systems, or portions of systems, that are not classified as high energy.

Nuclear island

Consists of a reactor module, its support building and operation center.

Pipe whip

Rapid motion of a pipe resulting from a circumferential or longitudinal break.

Restrained zone of influence (RZOI)

The three-dimensional space that encompasses the region swept out by the whipping pipe and the attached fluid jet cone or fan when the pipe motion is restrained by the presence of a whip restraint (WR), a barrier or a structure; or the region influenced by the jet cone or fan that is blocked by a jet shield, a barrier, or an intervening structure.

Rupture

The process or instance of breaking open.

Static plastic hinge

The location of plastic deformation due to pure bending with loads applied statically.

Unrestrained zone of influence (UZOI)

The three-dimensional space which encompasses the region swept out by an unrestrained whipping pipe and its fluid jet cone or fan.

Terminal end

That section of piping originating at a structure or component (such as a vessel or component nozzle or structural piping anchor) that acts as an essentially rigid constraint to the piping thermal expansion. Typically, an anchor assumed in the piping code stress analysis would be a terminal end. The branch connection to a main run is one of the terminal ends of a branch run, except for the special case where the branch pipe is classified as part of a main run. In-line fittings, such as valves, not assumed to be anchored in the piping code stress analysis, are not terminal ends.

Through-wall crack

A through-wall crack is assumed to be a circular orifice through the pipe wall of cross-sectional flow area equal to the product of one-half the pipe inside diameter and one-half of the pipe wall thickness (ANS, 1998).

Chapter 1

Introduction

1.1 Background

On June 9, 1985, a 760 mm hot reheat line bursts at Mohave Power Station, Laughlin, Nevada. The reheat line cycles steam back through the boiler stack after it has expanded through the high-pressure turbine and before it reaches the low-pressure turbine. A 1 000°C steam cloud blew down the door leading to the control room of the station, fatally scalding six workers (Young, 2010).

A pipe rupture occurred at Mihama, Japan on August 9, 2004, killing four and injuring seven people. The rupture was in the condensate system, upstream of the feedwater pumps. The carbon steel pipe carried 300°C steam at high pressure. The pipe had not been inspected since the power plant opened in 1976. In April 2003, a sub-contractor informed the owner that there could be a problem; an ultrasound inspection was scheduled but before the inspection could commence the superheated steam blew a hole in the pipe (Corrosion Doctors, 2011). The damage can be seen in **Figure 1**.

Figure 1 – Pipe rupture on a nuclear plant (Corrosion Doctors, 2011)

In response to these and similar accidents other power companies (with the same type of pipe design) were prompted to perform inspections of their pipes. Sixteen plants subsequently replaced their steam pipes (Corrosion Doctors, 2011).

Nuclear power plants have started to implement the American Society of Mechanical Engineers (ASME) section XI (ASME, 2004d) that guides the owner when inspecting all of the pressurized piping and the components, thus minimizing the risk of these types of accidents occurring. South African pressure equipment regulations include risk based inspections (RBIs) as stipulated in regulation 12 of the Occupational Health and Safety Act (85 of 1993) (South Africa, 1993). This inspection program is similar to the ASME section XI; albeit for non-nuclear and plant-specific applications. The inspection program's directive is to minimize the risk of fatal plant failures.

Piping in nuclear power plants on the nuclear island is designed, fabricated and tested to the stringent requirements of the ASME Boiler and Pressure Vessel code (ASME, 2004b). The auxiliary systems outside the nuclear island are designed, fabricated and tested to the requirements of the ASME code for power piping (ASME, 2004e).

The Nuclear Regulatory Commission (NRC) requires that nuclear plant safety be based on a defense-in-depth philosophy, and that protection against postulated piping accidents be provided by designing other protective features such as a pipe whip restraint for a pipe rupture event.

This research concerns a section of the nuclear power plant compliance with Part 50, Appendix A, GDC 4 of the United States Nuclear Regulatory Commission (USNRC) Code of Federal Regulations (CFR) which states (USNRC, 2005):

> *"Structures, systems, or components important to safety shall be designed to accommodate the effects of and to be compatible with the environmental conditions associated with normal operation, maintenance, testing, and postulated accidents, including loss-of-coolant accidents. These structures, systems, or components shall be appropriately protected against dynamic effects, including the effects of missiles, pipe whipping, and discharging fluids, that may result from equipment failures and from events and conditions outside the nuclear power unit. However, dynamic effects associated with postulated pipe ruptures in nuclear power units may be excluded from the design basis when analyses reviewed and approved by the Commission demonstrate that the probability of fluid system piping rupture is extremely low under conditions consistent with the design basis for the piping."*

One of the requirements for a safe nuclear power plant design is the postulation of the dynamic effects of a steam pipe rupture. The dynamic effects are the discharging fluid and pipe whip on structures, systems or components. A pipe rupture can occur in the steam pipe system where a defect such as a crack exists.

Multiple factors contribute to the initiation of pipe cracks during the plant's life. Cracks may start microscopically small and over time, with the assistance of cyclic operation, fatigue may elongate the crack. When a steam pipe is cooled by water during an accident, steam condensate may accumulate and form slugs of water. This water will have an effect on the system - termed condensation induced water hammer. Barna and Ezsöl (2011) performed experiments in the PMK-2 facility, which is a thermal hydraulic model of a nuclear power plant in Budapest, Hungary. Barna and Ezsöl (2011) indicated that the practical experiments have narrowed down the conditions for this event to occur but that a fulltime numerical simulation was not completed; further work in this field could be beneficial.

ASME has established non-destructive examination processes and procedures in section V of the Boiler and Pressure Vessel code. In this section the difference between a crack as an 'indication' and a crack as a 'defect' is defined (ASME, 2004c).

A crack as a defect is further defined and categorized as either a 'leakage crack' or a 'through-wall crack' (ANS, 1998).

In the case of a 'leakage crack' on a plant, the plant owner needs to decide the route to follow. The plant may be shut down and the crack can be repaired or the plant owner can initiate a monitoring program (ASME, 2004d) that allows the plant to be operated over a pre-defined timeframe during which the plant can be safely shut down. This methodology is termed 'leak-before-break' (LBB) (PennEnergy, 2011).

By applying the leak-before-break criteria a utility can prove to the regulatory commission (USNRC, 2005) that by means of extensive measures a pipe break accident is no longer considered. The concept of leak-before-break is still in the early development phase. Validation is also required before the regulatory commission (USNRC, 2005) may consider the criteria instead of applying the pipe whip criteria (PennEnergy, 2011).

The pipe rupture can be applied to any geometry or layout of a piping system. This geometrical or layout features can be an area of future study. Each layout can influence the forces and moments created by the rupture and different resultant forces can influence the final pipe whip restraint design.

During the period when a crack is monitored an event may occur at the plant, for example ‘condensation induced water hammer' on a main feedwater line (Barna and Ezsöl, 2011). This event may result in a pipe rupture that can be either a circumferential or a longitudinal break (ANS, 1998).

Nuclear power plant design must provide adequate protection against high-energy (HE) and moderate-energy (ME) fluid system pipe breaks. The integrity and operation of essential structures, systems or components (SSC) required to safely shut down the plant and mitigate the consequences of the piping failure must be ensured.

The logic of the pipe rupture evaluation procedure is shown in **Figure 2** (ANS, 1998). Considering the incidents at Mohave and Mihama power stations and applying the evaluation procedure shown in **Figure 2,** the first decision-diamond block indicates that the environment (D) needs to be considered. Taking the environment procedure further the evaluation includes target integrity. The control room door in Mohave plant would have been identified if this evaluation was performed prior to the evaluation procedure and the incident could have been prevented. Therefore calculations are performed to determine whether the plant requires additional protection during a pipe break event (ANS, 1998).

During the first stage of a pipe break the fluid thrust force will cause the pipe to deflect in an opposite direction than the fluid direction. The unrestrained zone of influence (UZOI) with regards to the hinge location will be used to determine the effect on the SSCs and the restraint position.

This research project is based on the development of a pipe whip restraint structure to protect the plant environment during a steam pipe break event in a nuclear power plant. It focuses on the structural component required to restrain the dynamic energy to an acceptable level.

A preliminary restrained zone of influence (RZOI) is also calculated. The intention is to envelop the zone of influence (ZOI) of a restrained pipe. If, during subsequent analysis, it is determined that a pipe whip restraint is required, the thrust force calculated during the RZOI analysis provides input to the restraint design.

The forces transferred to the wall via an overlay embedment plate during the event of the pipe break must be considered early in the design process. The overlay embedment plates are limited in their capacity to transfer large bending moments. Therefore, the design of the pipe whip structure must restrict the transfer of large forces and bending moments onto the overlay embedment plate (ANSI, 1994).

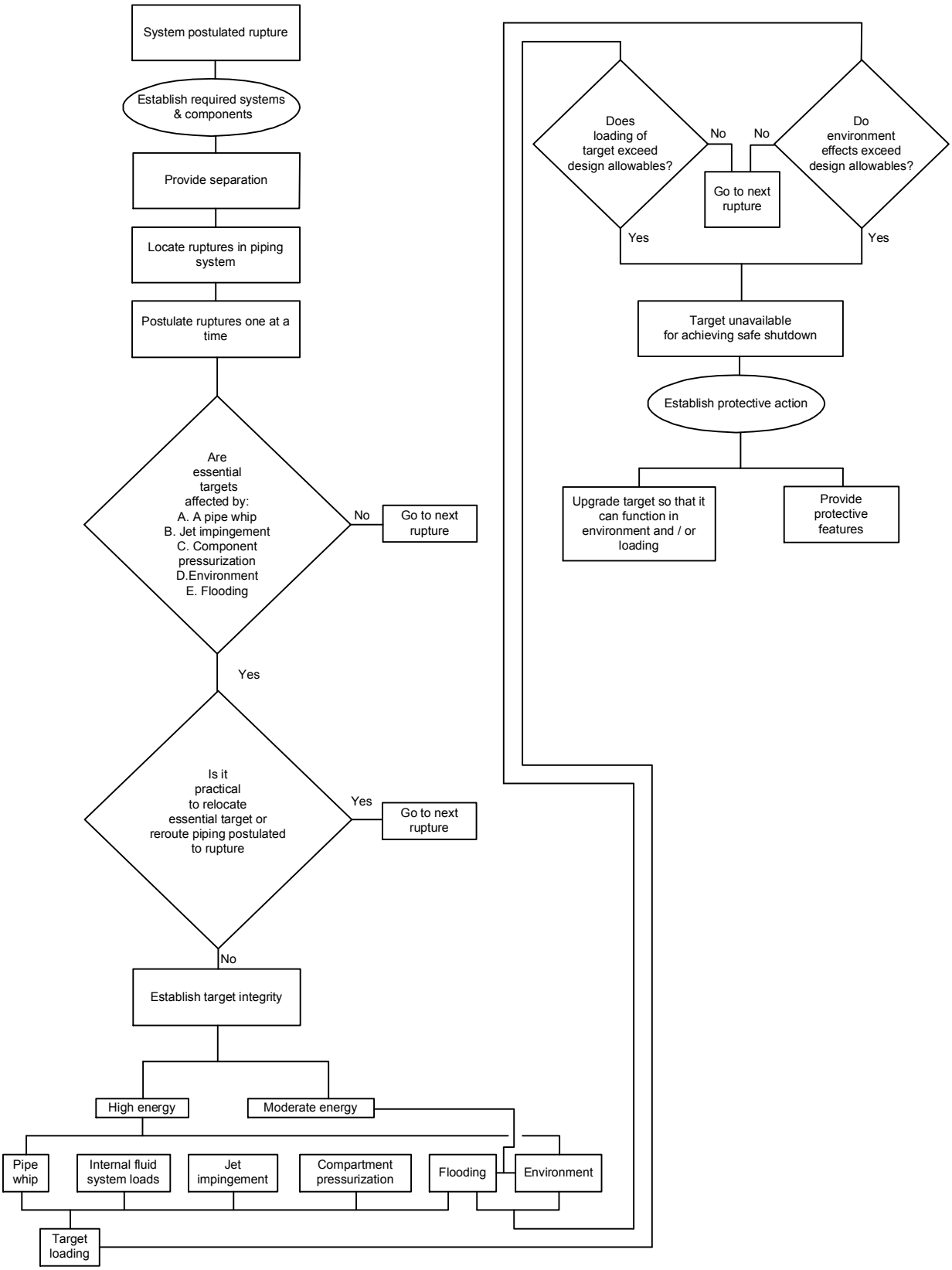

Figure 2 - Logic diagram for pipe rupture evaluation

During the last decades only a few pipe whip designs have been included in studies. Of these, very few have been implemented on-site. Leak-before-break has also been applied to gas and oil pipelines and pressure vessels (PennEnergy, 2011). Therefore, it would be an advantage to the petrochemical plants to consider pipe rupture on high-energy pipe systems.

1.2 Motivation of study

In order for plant owners/utilities (operating old nuclear power plants) to enhance or extend the life of their plant, they must receive a plant life extension license from the nuclear regulator. The regulator needs to be certain that no harm will come to the public. Part of the life extension motivation is a thorough service and inspection plan.

Also, designs such as AP1000® or EPR™ for new nuclear power plants require investigation of pipe rupture effects as part of the licensing process. The regulator has a duty to ensure that no harm comes to the public. This has resulted in additional requirements being placed on the owner: the implementation of the leak-before-break or the pipe break criteria on new plant design (USNRC, 2005).

The leak-before-break methodology uses intensive non-destructive examinations at frequent time intervals on thick-walled vessels and piping. The leak-before-break methodology is based on risk informed information (PennEnergy, 2011).

RBI has been developed in the last few years in the petrochemical field. RBI addresses the service situation of the plant components via non-destructive testing. Patel (2005) generated an inspection program for the Qatargas Company in which he discusses the levels of risk and the management thereof. Morisaki (2008) has developed software that supports the RBI program.

Both the nuclear and petrochemical inspection programs need to be approved by the regulatory body of the country or state. If the program is not approved, another methodology such as the pipe whip and restraint methodology is applied.

The pipe whip restraint has been applied to the nuclear plant environment and could be considered for the petrochemical plant environment as well, all dependent on the hazardous risk accompanied with the pipe rupture incident.

The pipe whip restraints instituted as part of this plant extension and new plant licensing process require thorough design and testing.

1.3 Research objectives

This dissertation focuses on the study of a pipe whip restraint during an unforeseen plant pipe rupture event of a high-energy (HE) pipe. These pipe whip restraints are installed within the plant area - normally against a wall or integrated into a structure, but not physically integrated into the process plant component or process system.

This dissertation will start off by explaining the methods used to calculate the forces followed by its application on a practical example of a pipe whip restraint. A specific plant environment will be assumed for the pipe whip restraint.

The overall objectives of this research project are as follows:

1. To apply a numerical design analyses philosophy to a break using the energy method.
2. To conceptualize design and evaluate the different pipe whip restraint designs.
3. To validate the pipe whip design with a dynamic finite element analysis.

1.4 Scope of the study

In order to meet the research objectives, this research will include the determination of the input values and characteristics for the objectives listed in **Chapter 1.3**. These input values and characteristics are:

Thrust force:

a. To determine the initial and steady-state thrust force for the break due to the upstream and downstream process influence.

Plastic hinge:

b. To determine whether a dynamic plastic hinge or static plastic hinge develops in the ruptured pipe and the effect on the pipe whip restraint design.

Pipe whip restraint geometry:

c. To determine the loads and sizing of different whip restraints due to the restraint geometry.
d. To determine the best restraint geometry for this application.

For the design of the pipe whip restraint, the following functional characteristics are applicable:

e. To avoid excessive impact loads on existing plant structures in the area of which the pipe break will occur.

f. To prevent impact damage to neighboring pipes and components critical to safely shut the plant down.

Assessment of the influence on the plant environment includes:

g. To avoid human access or interference during the pipe break operation.

h. To ensure that the structure is maintenance free throughout the plant life if a pipe break does not occur.

i. To design for a once-off operation.

Defects on welds are not considered for the purpose of this dissertation as they require immediate repair. The crack and indication on weld examination and the non-destructive examination processes are also excluded from this dissertation. The calculation - using fracture mechanics of the timeframe from which a crack initiates until rupture - is excluded from this dissertation.

The root-cause analyses of the pipe rupture are not addressed in this dissertation. A circumferential break at a terminal end will be considered.

The thermo-hydraulic thrust forces will be calculated by using the American Nuclear Society (ANS) 58.2 (ANS, 1998).

Two types of pipe whip restraints will be considered: the U-bar and the crush pipe. A simple evaluation of whip restraints will determine the final concept. The concept will be validated by a dynamic finite element analysis.

1.5 Layout of dissertation

Chapter 1 starts by giving an outline of the dissertation and defines the background, motivation, objectives and scope of the study.

Chapter 2 starts by discussing the inputs and characteristics required in this dissertation. It gives a brief history on criteria for postulating a pipe rupture and presents the different influences in determining the forces from the initiation of the pipe rupture to the resultant forces of this specific break.

Chapter 3 presents two conceptual designs that are considered for this specific pipe rupture, the evaluation of the options and the best concept for the application.

Chapter 4 demonstrates the validation of the design by means of a dynamic finite element analysis.

Chapter 5 concludes the dissertation and discusses research topics for further work.

Chapter 2

Literature review

During the design of a steam pipe whip restraint, analyses of forces and bending moments are required for each specific pipe rupture. The method of calculation of the forces and bending moments required to effectively design the pipe whip restraint are discussed first. This information will be used during further analysis to determine the center of the pipe whip restraint so that the effect of energy absorption is maximized.

2.1 Pipe rupture location

In a nuclear power plant a pipe is routed from one component to another, for example, from a heat exchanger to a boiler (ASME, 2004b). The criteria for postulating specific rupture points are provided by the American Nuclear Society for class 1 piping (ANS, 1998). These rupture locations are classified into two groups. The first is the terminal ends and the second is the high-stress intermediate locations of the piping system.

The position of a typical terminal end is indicated in **Figure 3**.

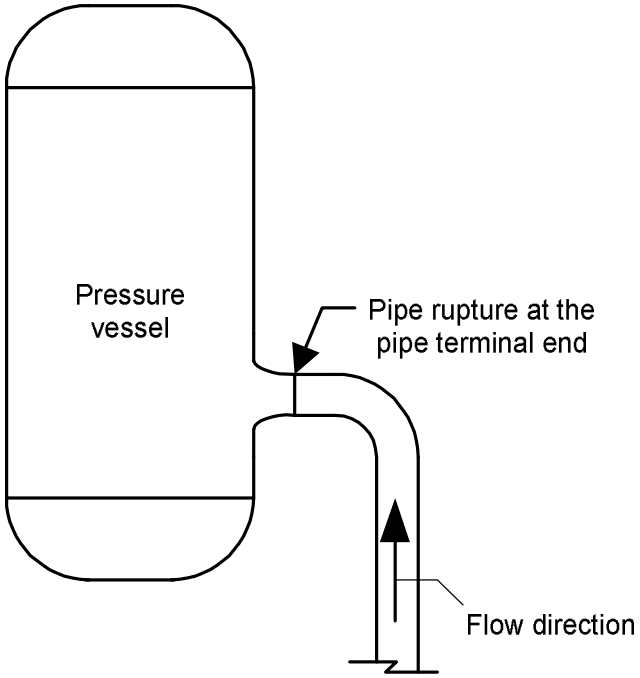

Figure 3 – Pipe rupture location

A circumferential pipe break can be influenced by the plant environment. Any structures or components in the vicinity of the break can influence the break and result in a limited separation break as indicated in **Figure 4**.

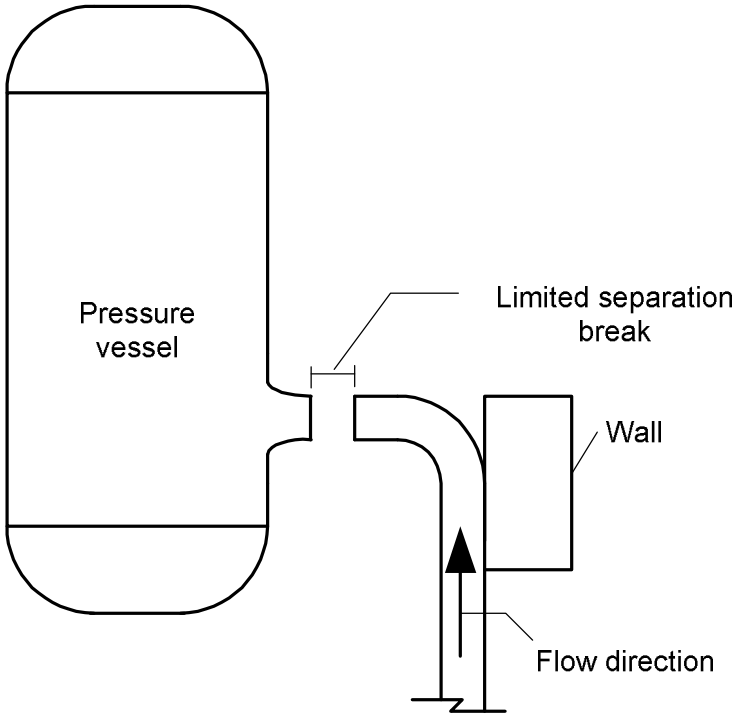

Figure 4 - Limited separation circumferential break

The plant environment for the pipe rupture analyzed for the purpose of this dissertation does not have any obstructions close to the break; therefore, a full separation circumferential break will be considered (ANS, 1998). To fully comprehend the forces a break plane is defined that will divide the break into an upstream- and a downstream break plane. Note that the direction of normal fluid flow determines the upstream and downstream sides of the break. **Figure 5** illustrates the break plane.

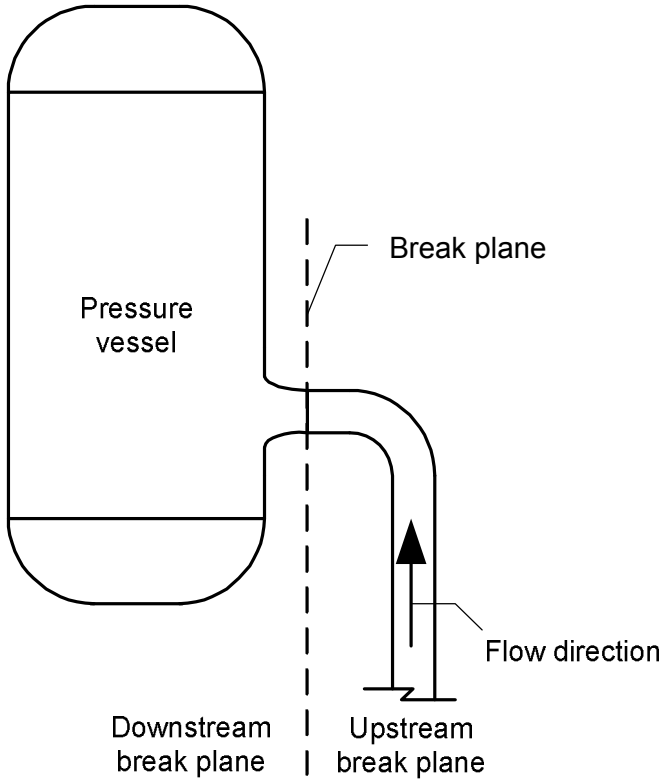

Figure 5 - Pipe break plane

2.2 Operating conditions

The American Nuclear Society specifies that the operating conditions used during the analysis must be determined by one of the following criteria (ANS, 1998):

> *"(a) For those portions of piping systems normally pressurized during operation, the thermodynamic state in the pipe and associated reservoirs shall be that corresponding to 100 percent power.*
>
> *(b) For those portions of high-energy piping systems which are normally pressurized only during plant conditions other than 100 percent power, the thermodynamic state and associated operating conditions shall be determined using the most severe mode."*

The system under investigation will be pressurized during normal power operation (100% power). The pipe internal fluid conditions used are:

Pressure:	5770.91 kPa (absolute)
Temperature:	273.05°C
Fluid:	Water

The pipe used:

Pipe details:	150NB Schedule 160 (ASME, 2004f)
Pipe material:	ASME SA-333 Grade 6 (ASME, 2004a)

2.3 Thrust force

2.3.1 Upstream break plane

The force for the upstream break plane is created by the pressurized fluid flow and is called the upstream thrust force (T_x). **Figure 6** illustrates the fluid flow and the thrust force (T_x).

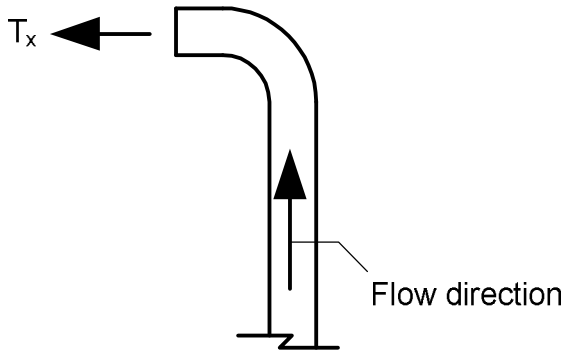

Figure 6 - Upstream fluid flow and thrust

The thrust generated by the fluid exiting the pipe is divided into two parts: the initial- and the steady-state thrust. The initial thrust is the maximum thrust from the time the break is generated, to the time when a full break is achieved. The force will increase from zero to a point where the flow is choked at the break plane (Moody, 1969).

Figure 7 shows the generic graph that the American Nuclear Society has adopted from the experiments performed by Moody (1969).

The second thrust force analyzed is that which is reached when a steady-state flow has been achieved and the reservoir conditions have reached the break plane. This assumes that the reservoir supplying the fluid remains at constant pressure (Moody, 1969). The American Nuclear Society has adopted this approach and included it in the pipe whip analysis guidelines (ANS, 1998). Moody (1969) used the steady-state thrust coefficient experimental two-dimensional data of the work done by Birkhoff and Zarantonello (1957) and Milne-Thompson (1963) and confirmed it mathematically.

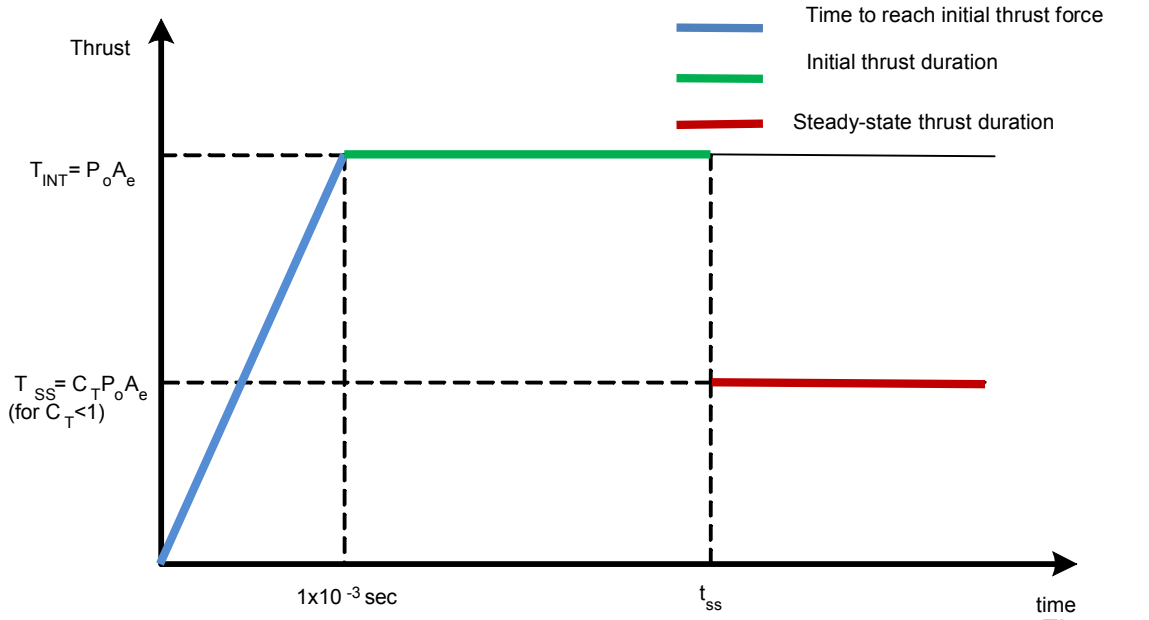

Figure 7

- **Typical thrust force time history**

Predictions of steady-state flow were made by Fauske (1962; 1965); Moody (1965; 1969); Henry (1970) and Henry and Fauske (1971). The American Nuclear Society evaluated these studies and found that Moody's study (1969) is the most conservative. Thus, the American Nuclear Society has included Moody's experimental data in the ANS 58.2 standard (ANS, 1998).

2.3.2 Downstream break plane

Due to the pipe break the high pressure in the vessel will force the fluid to exit the nozzle. **Figure 8** indicates the fluid flow direction of the downstream plane. A jet of fluid will stream out of the vessel at a high velocity. The presence of any object in the area of the jet stream will result in fluid forces being directed onto that object. These fluid forces will influence the design of the pipe whip restraint if it is situated in the proximity of the jet stream.

The jet geometry model, as sketched in **Figure 9** and adopted by the American Nuclear Society (ANS, 1998), is based on the experimental work performed by Moody (1969).

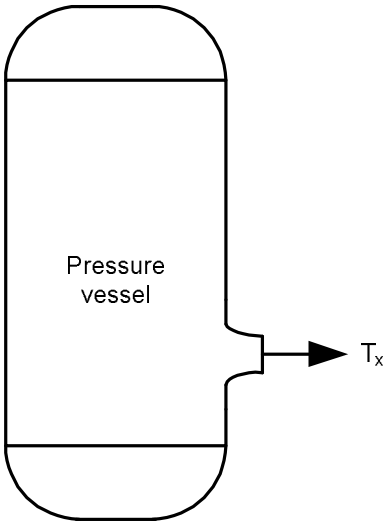

Figure 8 - Downstream thrust (T_x)

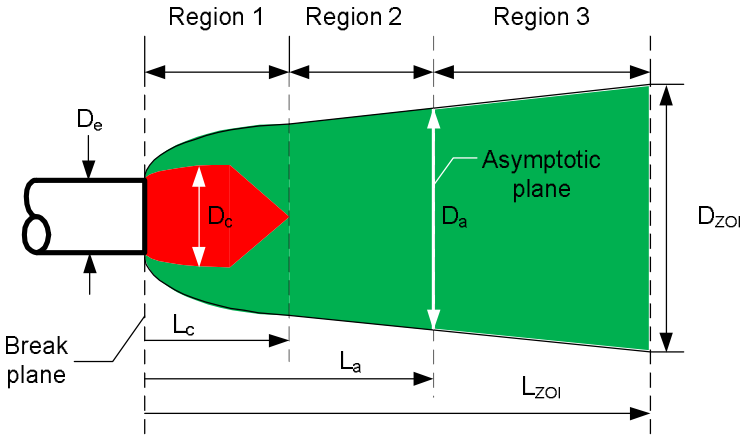

Figure 9 - Sketch representing expanding jet geometry

Jet region 1 is the jet core region. The whip restraint should preferably not be placed in this region because it will experience the highest jet impingement force. Jet region 2 is where the jet expands to the asymptotic plane. Jet region 3 is the zone of influence where components may be placed.

The dimensions for the jet-spray geometry are provided in ANS 58.2 (ANS, 1998) where D_e is the inside diameter of the process pipe. For jet region 1, D_c is the core diameter and L_c is the core length. For jet region 2, D_a is the jet diameter at the asymptotic plane and L_a is the distance from the break plane to the asymptotic plane. For jet region 3, D_{ZOI} is the zone of influence diameter and L_{ZOI} is the zone of influence length.

The thrust force applicable to the pipe whip restraint is a combination of the pipe whip force and the jet impingement forces. **Figure 10** illustrates the forces on a pipe whip restraint, comprising T_{PIPE}, the force of the whipping pipe on the restraint; and T_{JET}, the force of the jet on the restraint.

If a pipe whip restraint is installed in the area indicated in **Figure 10**, this restraint will be influenced by a jet impingement force that must be included in the design load conditions.

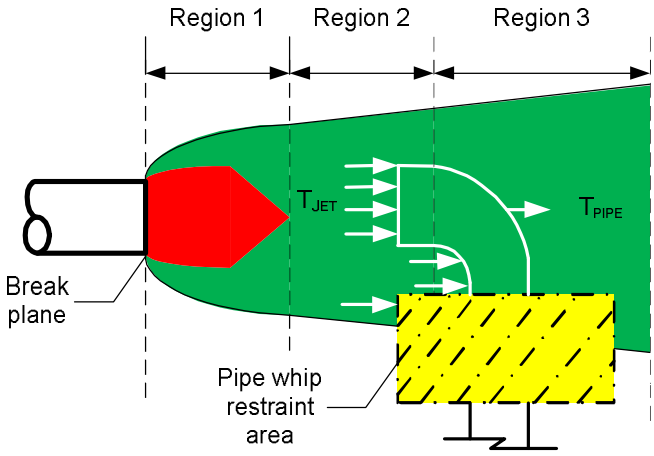

Figure 10 - Summary of all forces influencing the design

The American Nuclear Society has adopted the research done by Weigand (1983). ANS 58.2 (ANS, 1998) allows the analyst to determine jet impingement loads in each region and use these loads for the design of the systems, structures or components that will be influenced by these jet impingement loads. The study is based on the momentum equations and is used to describe the jet blow-down force on structures such as pipes, H-frame beams, angle iron webs, and so forth. The American Nuclear Society's tests have resulted in shape factors for each type of structure form that allows the simplification of complex structures to assist in the calculation of jet impingement force on a structure.

2.4 Hinge determination

At the initiation of a rupture, the inertial effects may result in plastic deformation in the mid-span of the pipe, or at a location of reduced moment capacity such as an elbow (Roemer and East, 1980). A dynamic hinge separates the whipping section from the rest of the structure. If a dynamic hinge forms the whipping section is assumed to be localized to rotation about the hinge (Roemer and East, 1980).

A dynamic hinge point is indicated in **Figure 11** for plastic deformation at mid-span of the pipe.

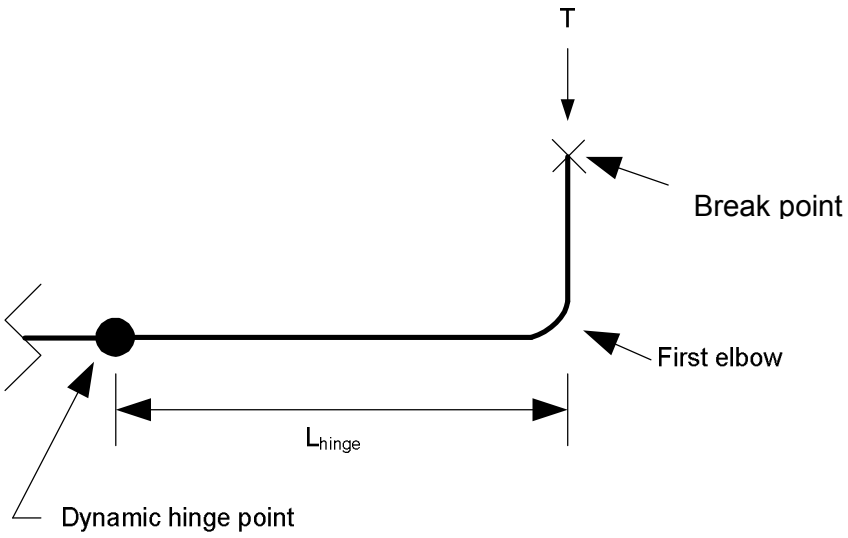

Figure 11 – Dynamic hinge point

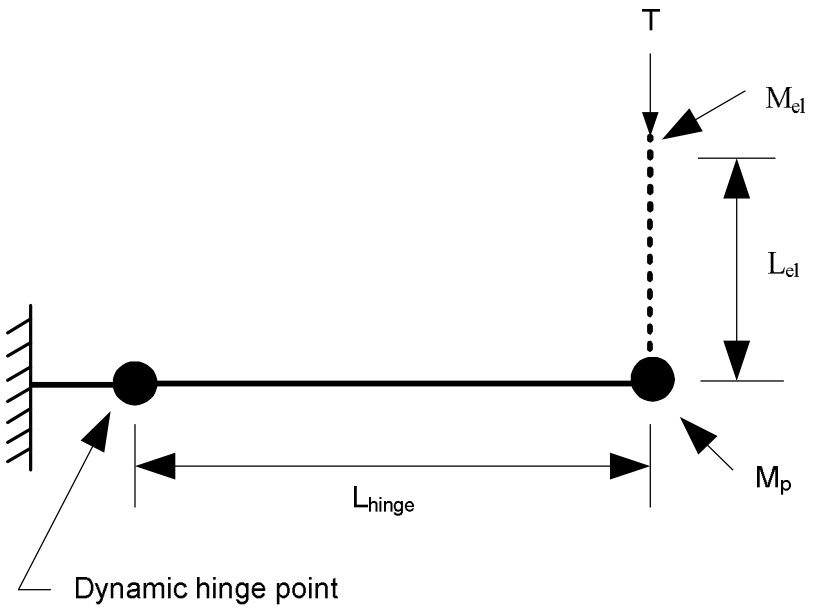

Figure 12 – Typical rigid plastic structure

If no dynamic hinge forms the loads are considered to be applied statically to a rigid, perfectly plastic structure as indicated in **Figure 12**. The first section of the pipe up to and including the pipe bend is considered as being subjected to a point load (M_p). Although the event is dynamic, and the forcing function is similar to a step input, no dynamic load factor is applied to the load when it is considered statically. Otherwise, this would tend to reduce the

lengths required to form a plastic hinge and reduce the associated zone of influence (Roemer and East, 1980).

The duration of the initial thrust force is short, typically less than one second. If a dynamic hinge does not form, plastic deformation would first occur at the location of the maximum moment, or at a location where the moment-carrying capacity is reduced, such as at an elbow or a bend. In cases where a piping segment undergoes combined loading, such as bending and torsion, only the bending component of the load is considered in determining the hinge location. The combined loading would tend to increase the overall stress level, reducing the hinge length. If no plastic hinge occurs, the piping responds elastically (Roemer and East, 1980).

The determination of the behavior and position of the plastic region is the key to postulating the motion and impact of the ruptured pipe. The methodology for determining whether a dynamic plastic hinge forms and the equation used to determine the hinge location was obtained from Roemer and East (1980). A 10% increase in the ASME section II code specified minimum yield strength (ASME, 2004a) was used per ANS 58.2 section 6.6.3 (b) (ANS, 1998). A fixed restraint within this length that is capable of withstanding the thrust force will result in no dynamic hinge formation (Roemer and East, 1980). The distance x in **Figure 13** must be less than the distance L_4 to ensure that no secondary hinge will develop.

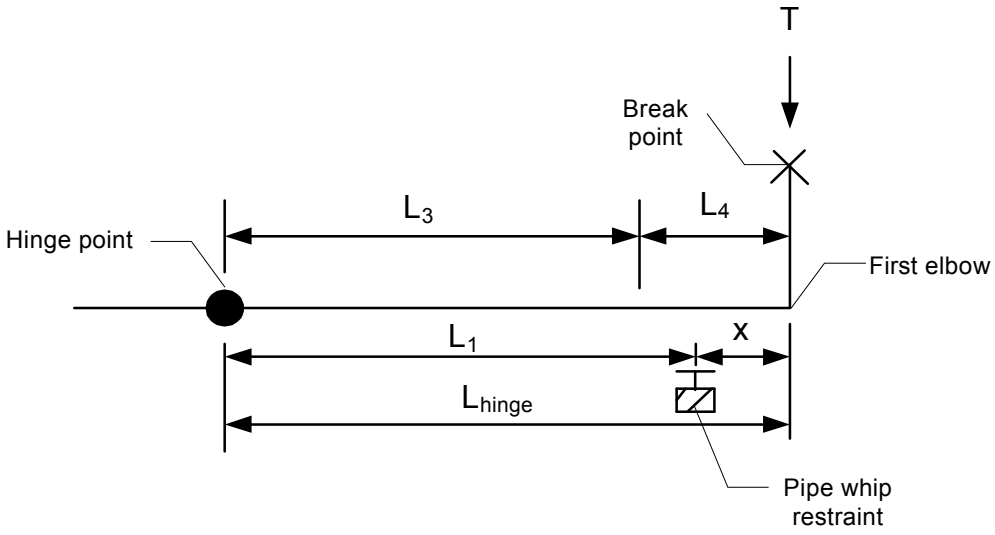

Figure 13 – Typical pipe whip restraint placement

A simplified closed-form solution has been developed by Vongmongkol, et al. (2011). Using this study the location of a pipe whip restraint can be determined to prevent a secondary hinge.

2.5 Pipe whip restraints

This section presents the concepts that are considered for the whip restraint. Honeycomb, U-bar and crush pipe are typical whip restraints used in the nuclear industry. These three design types have been the subject of numerous conceptual articles and papers at nuclear engineering conferences.

The USNRC has investigated the honeycomb concept via the information notice number 85-05 (USNRC, 1985) during which the material strength was not consistent during a test of different units of the same design. As a result the honeycomb concept will not form part of this dissertation but may be a subject for later study.

2.5.1 U-bar

The U-bar consists of stainless steel rods that are part of the assembly that absorbs the kinetic energy after a pipe rupture. The U-bar achieves energy absorption by undergoing considerable plastic deformation during the pipe whip event. By varying the diameter of the round bar, length of the round bar, and the number of U-bars placed parallel to each other, a wide range of energy absorption characteristics can be developed.

Experimental and analytical studies have been performed by the Department of Nuclear Safety Research in Japan (Miyazaki, et al. 1983). The conclusion of these studies was that the simple design formulas used were very close to analytical and practical results. The U-bar will only be designed using the formulae discussed in this dissertation.

Figure 14 depicts the typical structural components of a U-bar pipe whip restraint. A catch plate is provided to distribute the contact load between the pipe and round bar, bent in a u-shape and termed a U-bar, over a wide area. The clevis, pin and bracket arrangement at the attachment end provides in-plane rotation restriction capability. Adjustment capability is provided by the threaded clevis fitting to adjust the length as required by the design. Attachment of the assembly to the support structure is accomplished by welding the bracket to the sub-structure.

The clevis, pin and bracket arrangement can only be designed with elastic material properties whereas the straight section of the U-bar will be designed using plastic material properties.

The preliminary analysis of U-bars is based on the energy balance method and will be used in the concept design (Boresi and Schmidt, 2003).

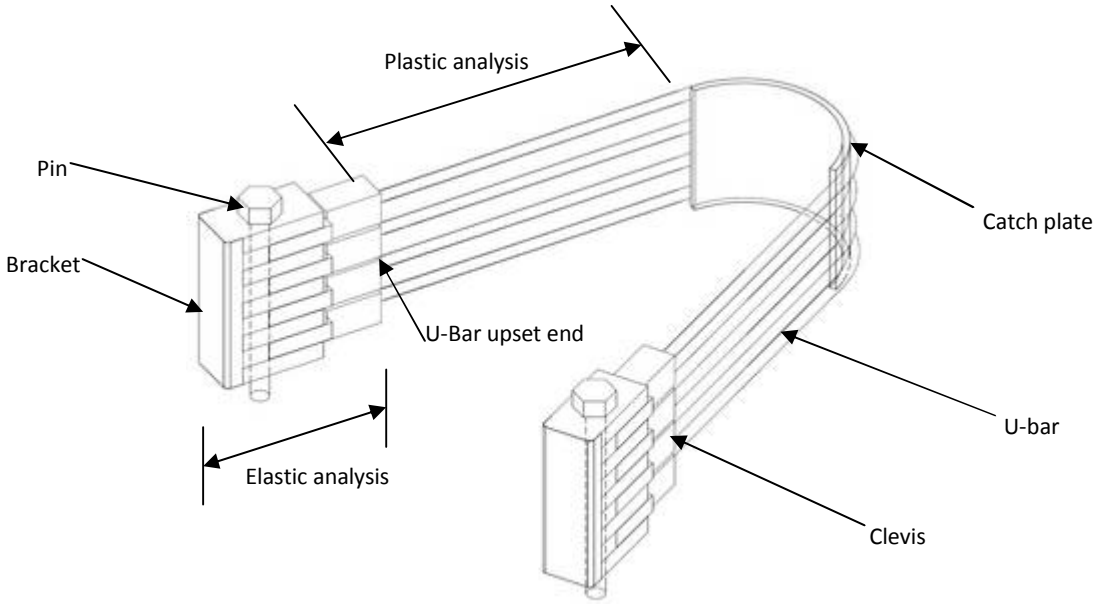

Figure 14 - U-bar restraint

2.5.2 Crush pipe

The crush pipe (CP) restraint consists of a short section of the B36.10 standard pipe (ASME, 2004f) that is placed perpendicular to the process pipe and at a longitudinal axis perpendicular to the plane of pipe movement. The standard pipe section is the part of the assembly that absorbs the kinetic energy after pipe rupture and typically undergoes considerable plastic deformation during the pipe whip event (Peach, et al. 1977; Spada and Goldstein, 1980). By varying the diameter and thickness of the pipe, a wide range of energy absorption crush pipes can be predetermined.

Figure 15 depicts the typical structural components of a CP-type pipe whip restraint. The CP will only be used once; therefore the clips are used to place the crush pipe in position onto a bearing plate and for replacement of the CP after use. The bearing plate is attached to the overlay plate by clips and slots which will be used to adjust the structure.

The crush pipe was evaluated through practical experiments to determine the geometry that will achieve the required damping force (Peach, et al. 1977; Spada and Goldstein, 1980).

Yang, et al. (2009) investigated the dynamic response of a pipe-on-pipe impact event by performing practical experiments. Numerical simulations of these experiments were performed using LS-DYNA®.

Neither breakage, nor failure of the pipes was observed but valuable information regarding the numerical parameters of deformation was generated.

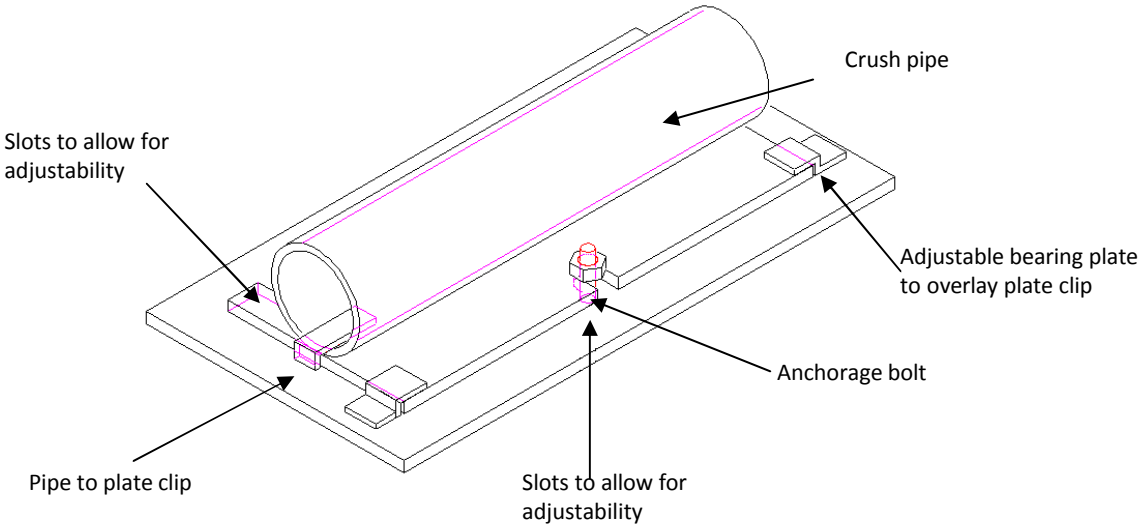

Figure 15 - Crush pipe restraint

2.6 Software

This dissertation will focus on a simple method to design the pipe whip restraint. The verification of this method will be performed by applying analysis code. The analysis codes used today have been developed over a period of time. The verification thereof is discussed in **Chapter 4**.

The force computation method discussed in **Chapter 1** and referenced as the Moody method has been programmed as part of the GETTO computer code (Bisconti, et al. 1975). Bisconti, et al. (1975) proposed a listed design code, GETTO1, and the example provided started with the equivalent resultant force as an assumed input. Although no practical experiments were performed, they implemented the information from suppliers to formulate this computer code.

Voros, et al. (2002) used the non-linear finite element analysis program COSMOS/M to model and analyze a pipeline. The results obtained for the expanding jet model indicate that the model explained in **Chapter 2.1** is conservative.

The behavior in the event of the hinge formation during the whip of the pipe can be analyzed by using the program ADINA. Experiments were conducted using the pipe diameter and the wall thickness ratio of the process pipe that breaks, whips around the hinge and impacts on another process pipe. The results of these experiments show that the strain limit in the process pipe under pressure was not reached regardless of the loading from the pipe break (Charalambus and Labes, 1993).

Biscontiet al. (1976) used the FRUSTA code to verify the GETTO code. They concluded that the limitation of the GETTO code is that it does not include all the phenomena that such a pipe break can display.

Lee and Koh (1995) performed an experiment and an analytical verification. A U-bar was tested and the results obtained compared to computer code ABACUS. During the study it was verified that the analysis is more conservative than the experiment. Thus, analysis proves to be an acceptable method for designing a U-bar restraint for a pipe break event and support to **Chapter 2.5.1** for design work performed in **Chapter 3**.

Engineers from Siemens used the ADINA code on nuclear power plant units for the main steam and main feed water lines (Andersen, et al. 2001). In the Anderson design the concept differs from that presented in this dissertation, but the criteria followed are the same. The analysis and detail design proved to be a solution for pipe break.

Ma and Bathe (1976) used the ADINA code to formulate a level 1 and level 2 type analysis. This includes both the pipe whip and the pipe-restraint analysis. The detail of the analysis has not been practically tested or verified. The analysis used one-dimensional analytical methods to better understand the pipe whip and its phenomena. Ma and Bathe's final study was conducted using two-dimensional analytical methods.

The U-bar restraint design was evaluated and compared to a practical experiment by Koh and Lee (1993). For comparison, the ANSYS code with ADLPIPE was used and the results compared to a practical experiment. The results indicated that the analysis is more conservative than the experiments and that the analysis is a safe computational model for designing whip restraints in **Chapter 3**.

The software available to the author is ANSYS-supported LS-DYNA® and the pre-processing will be performed using LS-PrePost®. Since a precedent was established by Koh and Lee (1993) through the ANSYS-supported analysis, and all other finite element analyses were shown to be more conservative than experimental data, it was deemed acceptable to use this code.

Yang, et al. (2009) used LS-DYNA® to model the impact action. The focus was on the deflection of the pipe but further work is required to evaluate the structural and material parameters of such a scenario or event.

Reid, et al. (2011) used the ABAQUS code to investigate the three-dimensional out-of-plane deformation of a failed pipe. During this study no pipe whip restraint was introduced. It could be seen that a large area was affected, therefore the need for a pipe whip restraint was envisaged.

Calonius (2009) studied different ways to model the pipe using ABAQUS. He did not include the effect of hydrodynamics in his problem. The shell element model with dense mesh is well compared to other models and studies. With limited plant parameters Calonius' model is a good basis to start an extensive model using all plant parameters.

Calonius (2010) took his earlier work (Calonius, 2009) and improved the parameters of the analysis. He found that the plastic hinge still occurred at the restraint position. The inner pressure of the pipe and the seismic activity were included in this analysis. Good reporting on the energy balance was provided. Force and time graphs were also included.

The analysis field started early with a one-dimensional analysis; no practical experiments have been used to verify the study (Bisconti, et al. 1976), (Voros, et al. 2002). The analysis software ABAQUS, LS-DYNA®, GETTO and FRUSTO have all been used in evolutions of different aspects of the pipe rupture or pipe impact dynamic analysis. These studies included practical experiments but the simplified formula-based method for a pipe crush pipe was included in these studies.

2.7 Conclusion

This chapter presented the requirement from the American Nuclear Regulatory Commission and the process to eliminate certain break conditions. The principal engineering methodology of the pipe break analysis was indicated and simple methods that were validated for use in the nuclear industry were reported. These simplified methods are used to determine the conceptual designs of the whip restraint structure in the next chapter.

It was shown that the American Nuclear Society has adopted multiple areas of work performed by engineers in the nuclear industry.

Based on the articles which indicate the simplified methods, the forces and moments are used to determine the conceptual design of the whip restraint. The upstream and downstream conditions are taken into consideration and where applicable both need to be included to envelop the total effect of the pipe break condition.

The movement of the pipe during a pipe break creates a hinge and determining this position is critical to the placement. The method has been discussed and will be used in the next chapter.

The common pipe whip restraints were discussed and will be used to evaluate the best type of restraint for the problem used in this dissertation.

The development of different modeling techniques using three-dimensional numerical analysis (Calonius, 2010) for a dynamic pipe break from one-dimensional analysis has been a long and difficult road (Bisconti, et al. 1976). The numerical analysis will be used to validate the conceptual design pipe whip restraint.

Chapter 3

Conceptual design

This section presents the conceptual design of the steam pipe whip restraint and will indicate the engineering methods applied. A whip restraint is unique to each plant position and application. The simplified method described in **Chapter 2** (from the point applied force to the pipe whip restraint) will make the concept design simple.

A conceptual design is the first phase of the engineering design where potential design philosophies are considered and rated against each other. The concepts that have the best rated result will be used in the basic design of the component where more detail loads and combination of loads will be considered. This section will only consider the concept stage of the design.

3.1 Thrust force

In **Chapter 2.1** it was assumed that the break type was a typical terminal end break where the vessel nozzle is welded to the pipe. In **Chapter 2.2** the operating conditions, pipe size and specification were defined. The next step is to determine the initial thrust force (T_{INT}) and steady-state thrust force (T_{SS}) for the upstream side of the break using equation (3.1) and (3.2) (ANS, 1998):

$$T_{INT} = P_o \times A_e \tag{3.1}$$

$$T_{SS} = C_T \times P_o \times A_e \tag{3.2}$$

Voros, Zsidi and Vigh (2002) also used equations (3.2) and (3.2) to establish the jet impingement load on the target or wall to evaluate the effects.

The calculation and definition of terms are shown in **Appendix A**. **Table 1** indicates the results of the upstream condition of the break.

Table 1 - Thrust force calculation results

Force	Symbol	Value	Unit	Reference
Initial thrust	T_{INT}	78.68	kN	Appendix A
Steady-state thrust	T_{SS}	98.34	kN	Appendix A

The forces are now known and the process will continue to the next design step. The jet geometry can now be determined. The jet geometry will indicate whether a jet force needs to be included in the force acting on the pipe whip restraint.

3.2 Jet-spray geometry

In **Chapter 2.3** the jet-spray geometry was shown. The dimensions for the geometry can now be determined by using the ANS 58.2 method and formulae (ANS, 1998). For jet region 1 the jet core diameter (D_c) is determined using equation (3.3); the jet core length (L_c) is determined by using equation (3.4) (ANS, 1998).

$$D_c = \sqrt{C_{Te}} \left(1 - \frac{L}{L_c}\right) D_e \tag{3.3}$$

$$L_c = \left(0.26 \times \frac{\sqrt{\Delta T_{sub}}}{\sqrt{1K}} + 0.5\right) D_e \tag{3.4}$$

To determine jet region 2 the asymptotic area ratio (A_R) [equation (3.5)] must be determined first. The asymptotic area ratio (A_R) is read off Figure C-4 of ANS 58.2 (ANS, 1998).

$$A_R = \frac{A_a}{A_e} \tag{3.5}$$

The jet diameter of the asymptotic plane (D_a) is calculated using the area of a circle. The break plane to asymptotic distance (L_a) can now be determined by using equation (3.6) (ANS, 1998).

$$L_a = \frac{1}{2} \times \left(\sqrt{\frac{A_a}{A_e}} - 1\right) \times D_e \tag{3.6}$$

The zone of influence is the volume that could potentially have equipment situated within it. The zone of influence diameter will be calculated with the area of a circle after the zone of influence area (A_{ZOI}) has been determined by equation (3.7). The zone of influence length (L_{ZOI}) is the distance to the component or structure in the spray path. For the purpose of this dissertation the L_{ZOI} will be the distance to the building wall in the spray direction.

$$A_{ZOI} = \left[1 + \frac{2 \times (L_{ZOI} - L_a)}{D_a} \times \tan 10°\right]^2 \times A_a \qquad (3.7)$$

These calculations have been performed in **Appendix A** and the results are shown in **Table 2** (**Figure 9** indicates the dimensions).

Table 2 - Jet-spray geometry calculation results

Dimension	**Symbol**	**Value**	**Unit**	**Reference**
Pipe inside diameter	D_e	131.75	mm	Appendix A
Jet core diameter	D_c	147.89	mm	Appendix A
Jet diameter at asymptotic plane	D_a	872.44	mm	Appendix A
Zone of influence diameter	D_{ZOI}	1206.46	mm	Appendix A
Core length	L_c	65.88	mm	Appendix A
Length to asymptotic plane	L_a	370.34	mm	Appendix A
Zone of influence length	L_{ZOI}	1317.50	mm	Appendix A

With the jet-spray dimensions known the plant model can now be studied to evaluate whether the jet will spray onto the pipe whip restraint or not. This evaluation will indicate if the jet force needs to be added to the whip force to obtain a total force onto the pipe whip restraint.

3.3 Thrust force time history

The pipe thrust force will reach initial thrust force conditions almost instantaneously ($T_{INT} < 0.1$ s). The calculation in **Appendix B** shows that the pipe thrust force will change from initial thrust to steady-state thrust in 0.638 s (t_2). This is illustrated in **Figure 16**.

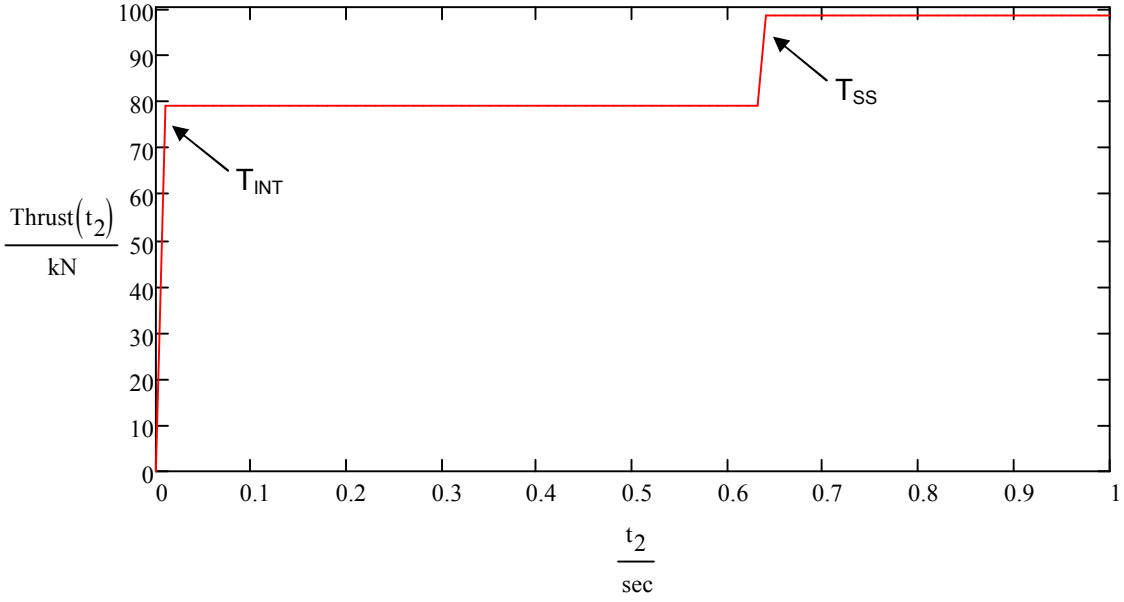

Figure 16 - Break thrust force time history

3.4 Hinge determination

In **Chapter 2.4** the dynamic and static hinges were explained. Now that the thrust forces are known the next step is to determine the dynamic and static hinge lengths. The dynamic hinge length can be determined by using equation 3.3 (Roemer and East, 1980):

$$L_{DH} = \frac{-\left(-3\cdot M_P\right) + \left[\left(-3\cdot M_P\right)^2 - 4\cdot(T)\cdot\left(-6\cdot M_P\right)\cdot\left(\frac{M_{el}}{m_p}\right)\right]^{0.5}}{2\cdot T} \tag{3.8}$$

The pipe whip restraint must be positioned so that no dynamic hinge or static hinge forms. The static hinge length can be determined by equation (3.4) (Micheli and Zanaboni, 2003). Vongmongkol et al. (2011) evaluated the simplified approach with a successful analysis:

$$L_S = \frac{M_S}{F_e} \tag{3.9}$$

The thrust force is used in **Appendix B** and **Appendix C** to determine the hinge length of the pipe. **Table 3** indicates the results.

Table 3 - Hinge length calculation results

Hinge length	Symbol	Value	Unit	Reference
Dynamic	L_{DH}	2.20	m	Appendix B
Static	L_S	0.29	m	Appendix C

With the hinge lengths known the different type of restraints can be calculated.

3.5 Equivalent thrust force

The higher magnitude force (*T*) is the larger force of either the initial thrust force or the steady-state thrust force. The equivalent trust force (F_e) at the restraint is determined by taking moments around the plastic hinge. **Figure 17** shows a simplified piping and whip restraint geometry. Consider the piping geometry as a simple supported beam with a cantilever load.

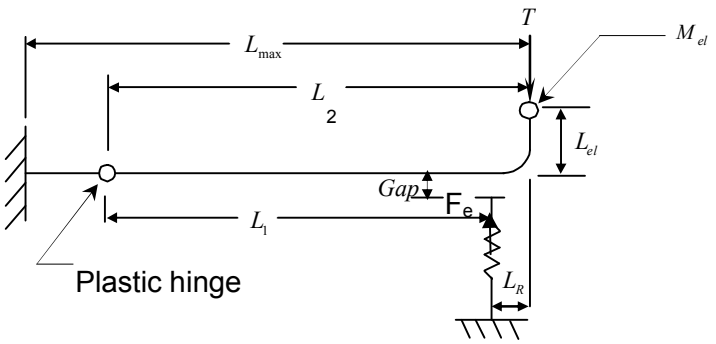

Figure 17 - Simplified piping and whip restraint geometry

Taking moments around the plastic hinge, equation (3.10):

$$T \times L_2 = L_1 \times F_e \tag{3.10}$$

A safety factor of 1.10 is introduced in equation (3.10) to account for rebound effects, resulting in equation (3.11) (USNRC, 1982).

$$F_e = 1.10 \times T\left(\frac{L_2}{L_1}\right) \tag{3.11}$$

3.6 U-bar concept

The U-bar pipe whip restraint concept design is calculated in accordance with the governing equations of the energy balance method (Micheli and Zanaboni, 2003; Inman, 2009).

$$\text{Internal work} = \text{External work} \tag{3.12}$$

$$F_e\,(G + d_t) = F_T \times d_t \tag{3.13}$$

The U-bar size has been determined in **Appendix C** and the results are summarized in **Table 4**:

Table 4 - U-bar calculation results

Result	**Symbol**	**Value**	**Unit**	**Reference**
Gap	-	0.05	m	Appendix C
Number of bars	n	4		Appendix C
Diameter of bars	d_{bar}	20	mm	Appendix C
Equivalent thrust resultant	F_e	244.08	kN	Appendix C
Transmitted load to back up support structure	F_T	705.28	kN	Appendix C

The force transmitted to the structure supporting the U-bar must be assessed by the structural engineer of the building. The wall must be able to withstand this force.

3.7 Crush pipe concept

The crush pipe whip restraint concept design is calculated using the governing equations of the empirical method (Peach, et al. 1977; Spada and Goldstein, 1980).

When the crush pipe is smaller or equal to the process pipe, equation (3.14) will be used:

$$L_{cp} = 2 \times D_b + D_p + 2 \times g_m \tag{3.14}$$

When the crush pipe diameter is larger than the process pipe, equation (3.15) will be used:

$$L_{cp} = 3 \times D_b + 2 \times g_m \tag{3.15}$$

The minimum wall thickness is calculated from equation (3.16):

$$t_{cp} = 0.75 \times t_p \times \left(\frac{r_b}{r_p}\right)^{0.131} \quad (3.16)$$

The load-crush or force of crush pipe (F_{cr}) deflection (δ) curve has been experimentally determined by the Welding Research Council's Bulletin 321 (WRC, 1987). The empirical scaling law has been included in this equation (Peach, et al. 1977; Enis, Bernal and Burdette, 1980). The total load F_c (3.17) can now be calculated:

$$F_c = F_{cr} + F_{ci} \quad (3.17)$$

The equations obtained from these experiments will be used to calculate three possible sizes for the crush pipes. These calculations are performed in **Appendix D** and the results are documented in **Table 5**.

Table 5 - Empirical design results

Pipe Size	**Crush Load (kN)**	**Reference**
100NB Schedule 120	882.46	Appendix D
150NB Schedule 120	1044.82	Appendix D
200NB Schedule 120	916.70	Appendix D

The empirical method calculated in **Appendix D** does not include the fluid energy within the process pipe, but only the load of the metal pipe. Therefore, this method is not suitable for this specific application. The loads in **Table 5** can therefore not be used in the design of the crush pipe type whip restraint.

Consider equation (3.12) again; this equation balances the internal work with the external work done, but the energy of the fluid has not been included. The author will now use the energy balance equation from the subject 'mechanics of materials' (Boresi and Schmidt, 2003) to include the energy of the fluid.

Consider the energy balance equation (3.18) in its basic form:

$$\text{Energy In} = \text{Energy Out} + \text{Losses} \quad (3.18)$$

The energy ‘in’ will be the strain energy (U_m) from the whipping pipe. The energy ‘out’ will be the potential energy of the crush pipe (U). From the energy equation (3.18) the specific energies identified are shown in equation (3.19) for the use in the crush pipe design.

$$\text{Strain Energy } (U_m) = \text{Potential Energy } (U) \tag{3.19}$$

The strain energy is the relation between the deformation and the force, which when presented on a force-versus-deformation graph the result of the area under the line will represent the energy (**Figure 18**). The deformation is dependent on the force applied.

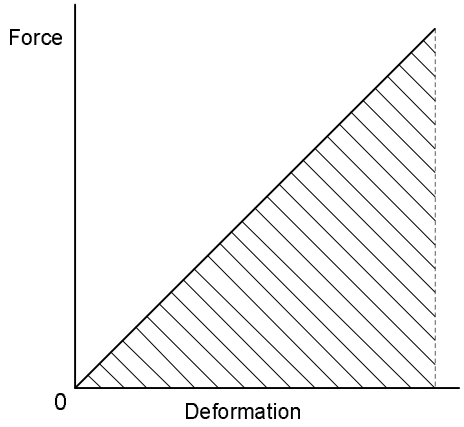

Figure 18 – Force against deformation graph

The strain energy (U_m) [calculated using equation (3.20)] for the whip restraint will be the higher magnitude force (T) over the plastic hinge distance (L_2), (see **Figure 17** for the simplified geometry).

$$U_m = ½ \times T \times L_2 \tag{3.20}$$

The potential energy (U) [calculated using equation (3.21)] will be the stiffness force (F_t) of the crush pipe over the distance from the plastic hinge to the pipe whip restraint.

$$U = ½ \times F_t \times L_1 \tag{3.21}$$

The stiffness force (F_t) [calculated using equation (3.22)] will be the product of the elastic ring stiffness (k_1) and the maximum deformation (δ_M) of the crush pipe plus the plastic ring stiffness (k_2) and the collapse deformation of the crush pipe (δ_C).

$$F_t = k_2 \times \delta_M + k_1 \times \delta_C \tag{3.22}$$

The strain energy and potential energy of the concept have been calculated in **Appendix E**. These results are summarized in **Table 6**.

Table 6 - Energy balance results

Pipe	Strain energy (kJ)	Potential energy (kJ)	Reference
150NB Schedule 160	268.49	Not applicable	Appendix E
250NB Schedule 80	Not applicable	288.95	Appendix E

The strain energy calculated is less than the potential energy of the 250NB Schedule 80 crush bumper pipe. Therefore, the energy method indicates that a 250NB Schedule 80 pipe bumper will be successful.

3.8 Pugh matrix

The concepts discussed in this chapter can now be weighed against each other to evaluate which concept will be the best suited to this specific application. The evaluation is done by using the Pugh (or decision) matrix (Wikipedia, 2011) based on Pugh (1981). The characteristics will now be discussed and followed with a summary table.

1. Avoidance of excessive impact loads on structures

   The function of the pipe whip restraint is to limit the movement of the whipping pipe to such an extent that no direct impact onto the structures is achieved. The U-bar and crush pipe designs will contain the whipping pipe and prevent any excessive impact loads on the plant structures such as walls and steel support structures.

   The U-bar concept and the crush pipe rate the same (S), see **Table 7**.

2. Prevention of impact damage to neighboring components

   The function of the pipe whip restraint is to limit the movement of the whipping pipe to such an extent that no direct impact onto the neighboring components is achieved - whether it is direct impact or transferred from the one pipe to another. The U-bar and crush pipe designs will contain the whipping pipe and prevent any impact damage on the plant components such as pressure vessels and piping systems.

   The U-bar concept and the crush pipe rate the same (S), see **Table 7**.

3. Maintenance free

A nuclear power plant is designed for a lifetime of forty years; during this time period maintenance is scheduled on components. The downside of maintenance is the loss of income during this period; therefore the pipe whip restraints must have a concept that is maintenance free.

The U-bar is of welded construction and the pin and bracket arrangement is permanently installed. Therefore, no additional maintenance is required. The crush pipe is of welded construction except for the clips and bolts that are used to locate the crush pipe in the final position. No maintenance is required on the crush pipe design; only inspection of the bolts and clips are required.

The U-bar concept and the crush pipe rate the same (S), see **Table 7**.

4. Once-off operation

The U-bar design is based on the round bar expanding into its plastic region during a pipe whip event; therefore the design can only be used once.

The crush pipe design is based on the pipe whip to deform or crush the pipe; therefore the design can only be used once.

Both concepts have to be replaced after a pipe break occurs. The U-bar concept and the crush pipe rate the same (S), see **Table 7**.

5. Transmitted load

The U-bar design will absorb energy during a break; the rest of the energy will be seen as a load and transmitted to the surrounding structures. The U-bar applicable to this concept is positioned so that the transmitted load is away from the wall creating a very large moment.

The crush pipe design will absorb the energy during the break; a small amount of energy will be transposed in the form of a load directly onto the wall. The crush pipe will have a small load compared to the moment of the U-bar design.

The crush pipe rate better (+) than the U-bar, worse (-). See **Table 7**.

6. Contained energy absorption

The U-bar design allows the designer to add or remove bar on the design. The flexibility in designs allows the energy absorption to be contained effectively.

The crush pipe design is limited to the pipe in the event of a break and does not have the flexibility to add material for better energy absorption.

The crush pipe rate worse (-) than the U-bar, better (+). See **Table 7**.

7. Support structure design

The structure on which the U-bar is being supported is of complex design for the current evaluation concept. Therefore, for a pipe that whips towards a wall the support structure will need to support the U-bar away from the wall creating a large moment from a small load after the energy absorption.

The crush pipe is of simple design for this concept as the pipe whips towards the wall. The support structure is very simple consisting of a few bolts and slots directly on the overlay plate.

The crush pipe rate better (+) than the U-bar, worse (-). See **Table 7**.

8. Compact design

The U-bar concept for this scenario is not a small compact design if you include the support structure, but more of a bulky design structure where the crush pipe is of very compact and simple design.

The crush pipe rate better (+) than the U-bar, worse (-). See **Table 7**.

9. Required overlay plates (OLPs)

The pipe whip will connect the pipe whip restraint; energy will be absorbed through the design of the pipe whip restraint. A support structure will keep the pipe whip restraint in position but the support structure will be anchored in the concrete floor or the wall of the building - this is performed by an overlay plate.

The current U-bar concept design will require a minimum of three overlay plates to accommodate the moment and torques loads from the pipe whip restraint.

The crush pipe design concept will require only one overlay plate due to the pipe whip towards the wall and the crush pipe can be placed in line with the whipping pipe.

The crush pipe rate better (+) than the U-bar, worse (-). See **Table 7**.

10. Plant layout

The plant layout of the selected pipe is such that when the pipe breaks it will whip towards the wall. The U-bar concept design will require a structure supported from the floor to the roof to support the U-bar in the opposite direction of which to whip takes place. This structure will require a complex design.

The crush pipe design concept will be placed on the wall. The pipe whips into the crush pipe where the load will be absorbed. This will be a simple design.

The crush pipe rate better (+) than the U-bar, worse (-). See **Table 7**.

Table 7 indicates the different measures, and the sum of negatives and positives that can be used to evaluate which design should be selected.

Table 7 - Pugh Matrix of the pipe whip restraints

Design Pugh Matrix		
Concept Selection Legend **Better +** **Same S** **Worse -**	**Concept 1 U-Bar**	**Concept 2 Crush Pipe**
Characteristic / Measure		
Avoidance of excessive impact loads on structures	S	S
Prevention of impact damage to neighboring components	S	S
Maintenance free	S	S
Once-off operation	S	S
Transmitted load	-	+
Contained energy absorption	+	-
Support structure design	-	+
Compact design	-	+
Required OLPs	-	+
Plant Layout	-	+
Sum of Positives	1	5
Sum of Negatives	5	1
Sum of Sames	4	4

The crush pipe design has five positive attributes with one negative attribute, whereas the U-bar has five negative attributes with one positive attribute. This indicates that, if the layout permits, the crush pipe design is better for this application than the U-bar.

3.9 Concept conclusion

The crush pipe is a simple design compared to the complex structure of the U-bar and where layout restraints permit, it should be used in preference to the U-bar. A concept determining factor for the type of restraint to be used is the direction of the whipping pipe motion: a whip towards the wall/structure will favor a crush pipe due to its simplicity; a whip away from the wall/structure will favor a U-bar restraint as the crush pipe is impractical to install. In the scenario analyzed herein, a crush pipe can be used.

The scenario shows that a large moment is generated with the U-bar design and that it acts on the wall, although the force is dampened through the bars. The potential energy of the crush pipe design results in less force transferred to the wall by the crush pipe.

Chapter 4

Concept validation

Chapter 2 discussed the theory of the pipe break and presented the applicable method to determine the jet force. Finite element programs are used today to accurately compute the forces of a pipe break. The program requires an understanding of the stress and the strain experienced during the pipe break. This chapter will discuss the analysis used in the nuclear field with reference to the pipe whip calculation.

4.1 Computer program: LS-PrePost®

LS-PrePost® is an advanced pre- and post-processor that is delivered with LS-DYNA® (LSTC, 2009). LS-PrePost® achieves fast rendering of data and XY plotting.

LS-DYNA® models can be generated and modified with the pre- and post-processor LS-PrePost®. The program is used to visualize the results of the LS-DYNA® Finite Element analysis. LS-DYNA® input files can be read in and editing of the keyword cards in the graphical user interface is possible.

For the purpose of this dissertation the keyword cards used are listed in Appendix F.

LS-DYNA® is an advanced general-purpose multi-physics simulation software package (LSTC, 2009). The package is capable of calculating many complex, practical engineering problems. Its origins and core competency reside in the non-linear transient dynamic finite element analysis using explicit time integration.

Non-linear in this context means at least one (and sometimes all) of the following apply (LSTC, 2009):

a. Changing boundary conditions (such as contact between components that change over time)

b. Large deformations (for example the crumpling of sheet metal parts)

c. Non-linear materials that do not exhibit ideally elastic behavior (for example thermoplastic polymers)

Transient dynamic means analyzing high speed, short duration events where inertial forces are important. Typical uses include (LSTC, 2009):

a. Automotive crashes (deformation of chassis, airbag inflation or seatbelt tensioning)

b. Explosions (underwater mines or shaped charges)

c. Manufacturing (sheet metal stamping)

4.2 Problem definition

The validation of the concept design as completed in **Chapter 3** requires an input file with piping parameters. The input file was created using LS-PrePost® with the pipe layout details as depicted in **Figure 19**. **Figure 20** shows the model generated in LS-PrePost®. **Figure 21** is an enlargement of the bumper area.

The pipe material was defined as ASME SA-333 Grade 6 in **Chapter 2**. This is a carbon steel typically selected for processes in the nuclear industry. The Young's modulus is 175.82 GPa (ASME, 2004a); the Poisson's ratio is 0.29 (ASME, 2004a); and the tensile yield strength is 173.06 MPa (ASME, 2004a). The pipe size is 150NB Schedule 160 (ASME, 2004f).

The initial thrust force (T_{INT} = 78.68 kN) and steady-state thrust force (T_{SS} = 98.34 kN) calculated in **Chapter 3** are used with the thrust force time-history graph (**Figure 16**), where the initial thrust will translate to a steady-state thrust .

The crush pipe is 250NB Schedule 80 (ASME, 2004f) and of the same material as the process pipe - ASME SA-333 Grade 6. The values have been summarized in **Table 8**.

Table 8 - Summary of input description and values

Input Description	Input
SA-333 Grade 6	Carbon steel pipe
Young's modulus of elasticity	175.82 GPa
Poisson's ratio	0.29
Tensile yield strength	173.06 MPa
Process pipe size	150NB Schedule 160
Initial thrust force	78.68 kN
Steady-state thrust force	98.34 kN
Crush pipe size	250NB Schedule 80

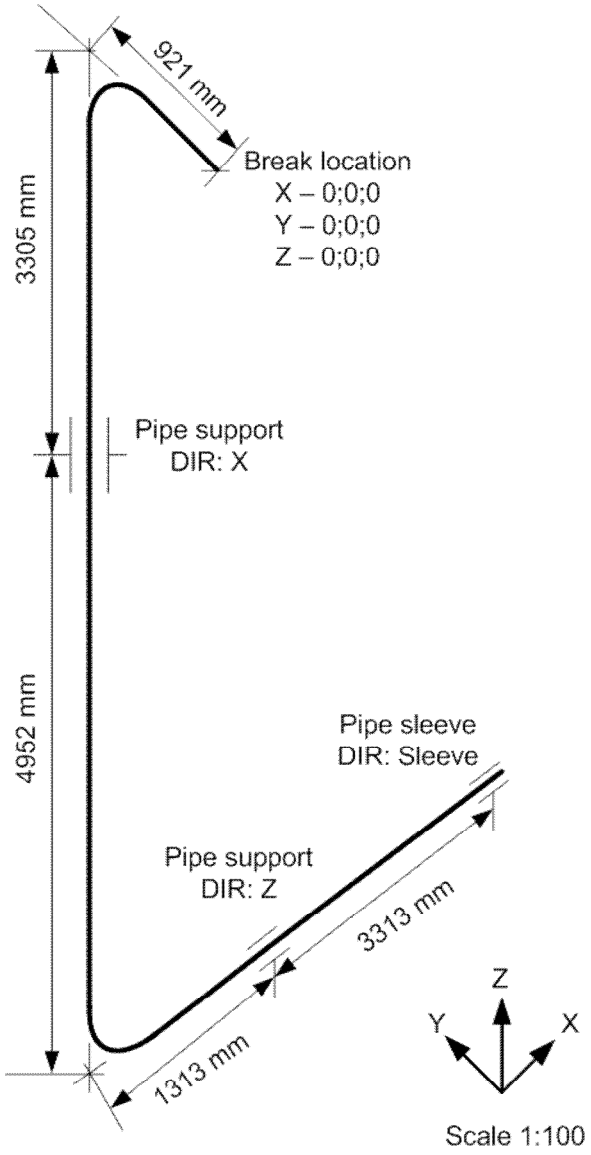

Figure 19 - Pipe layout

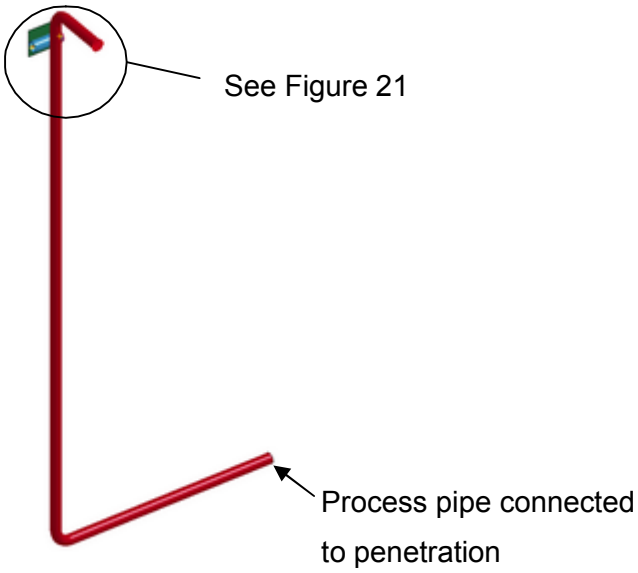

Figure 20 - The LS-DYNA® model of the pipe layout

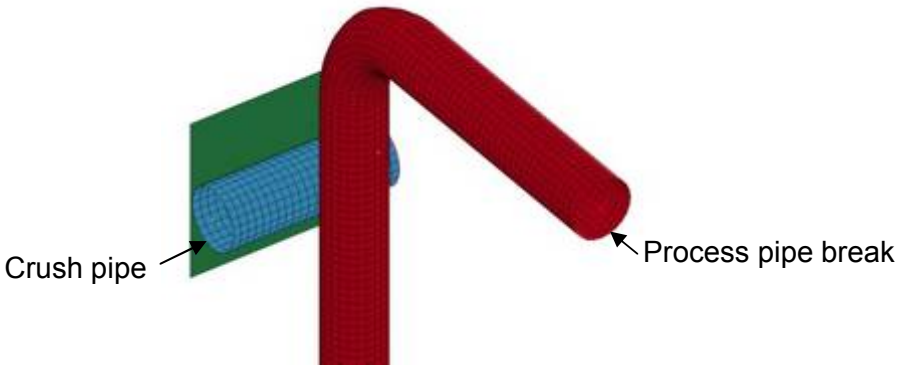

Figure 21 - The LS-DYNA® model of the crush pipe area

4.3 Dynamic hinge

The information from the LS-DYNA® simulation is processed with LS-PrePost®. The analysis starts with a time set at 0 s. **Figure 22** indicates the process pipe and the crush pipe before the analysis starts. The process pipe moves towards the crush pipe and after 0.019 s the initial impact is reached (see **Figure 23**).

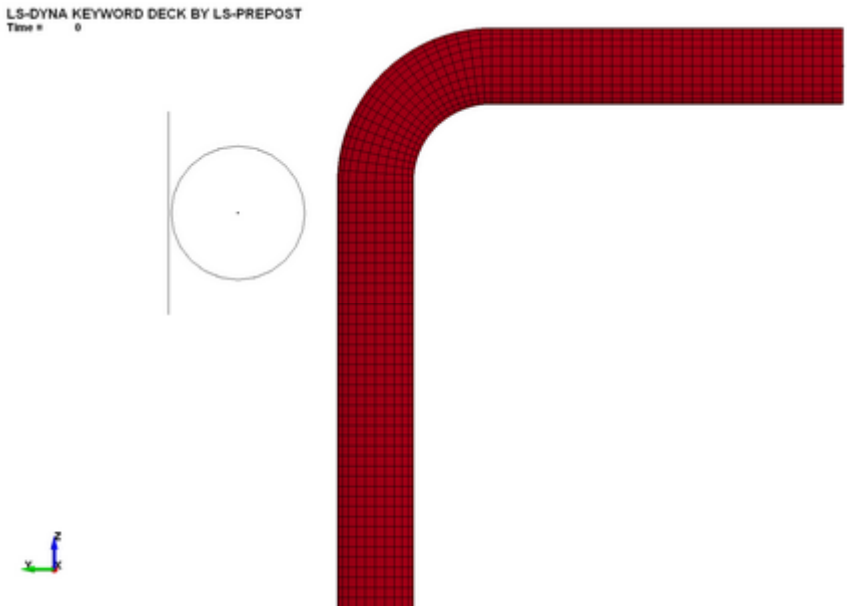

Figure 22 - The LS-DYNA® model at 0 s

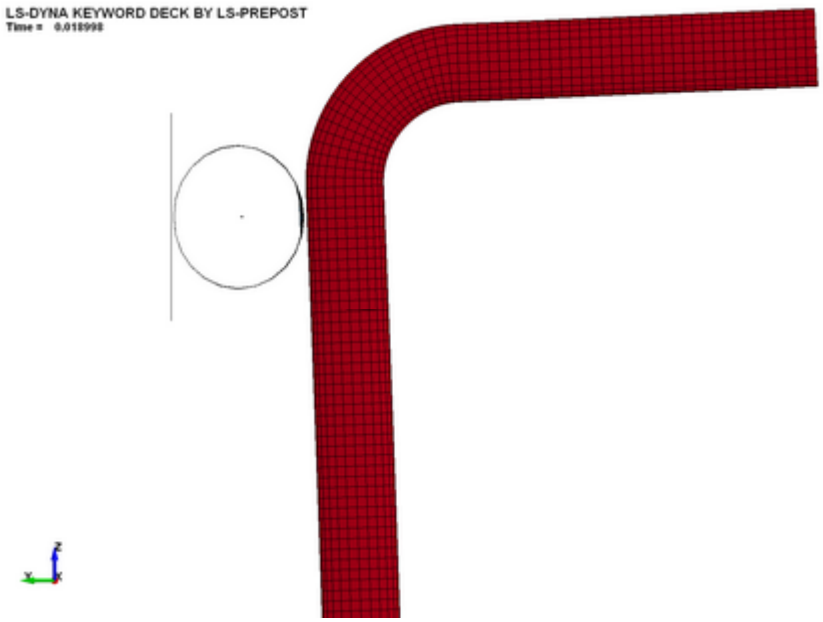

Figure 23 - The LS-DYNA® model at 0.019 s

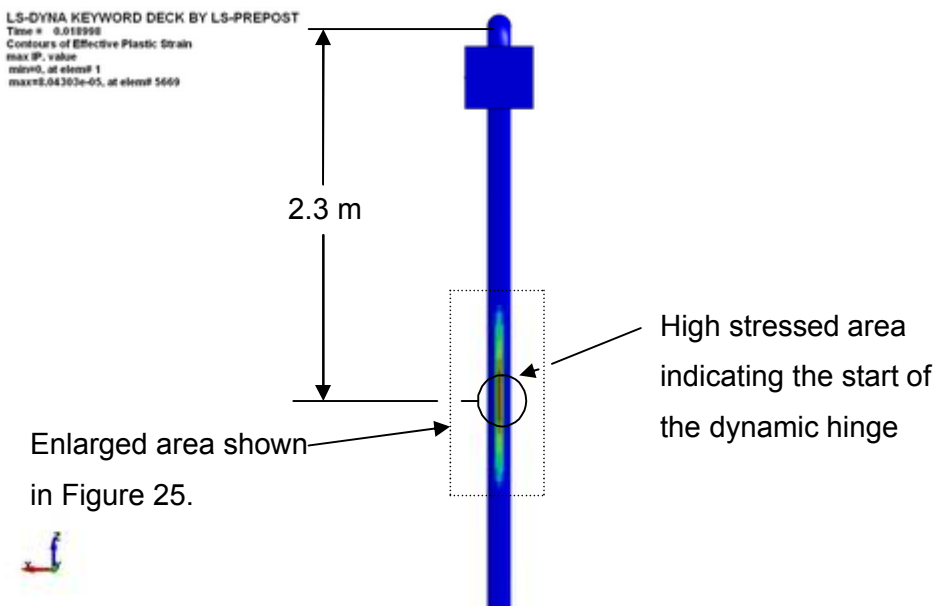

Figure 24 - The LS-DYNA® model of the dynamic hinge

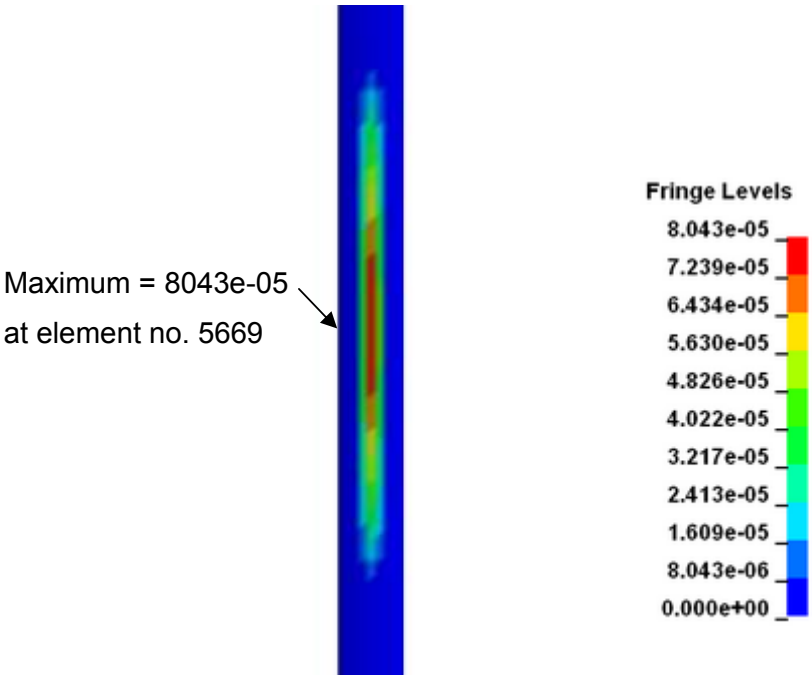

Figure 25 - The LS-DYNA® enlargement of the high-stress area

The dynamic hinge is shown in **Figure 24**. The dynamic hinge is formed at 2.3 m from the first elbow of the pipe. The fringe values in **Figure 25** indicate the high-stress area and the center is where the hinge forms before impact takes place on the crush pipe.

The velocity increase is at a very high rate but it also decreases at a very high rate after the break occurs. In **Figure 26** the first 0.15 s have been plotted on a graph, and from these results a wavelike phenomenon is generated.

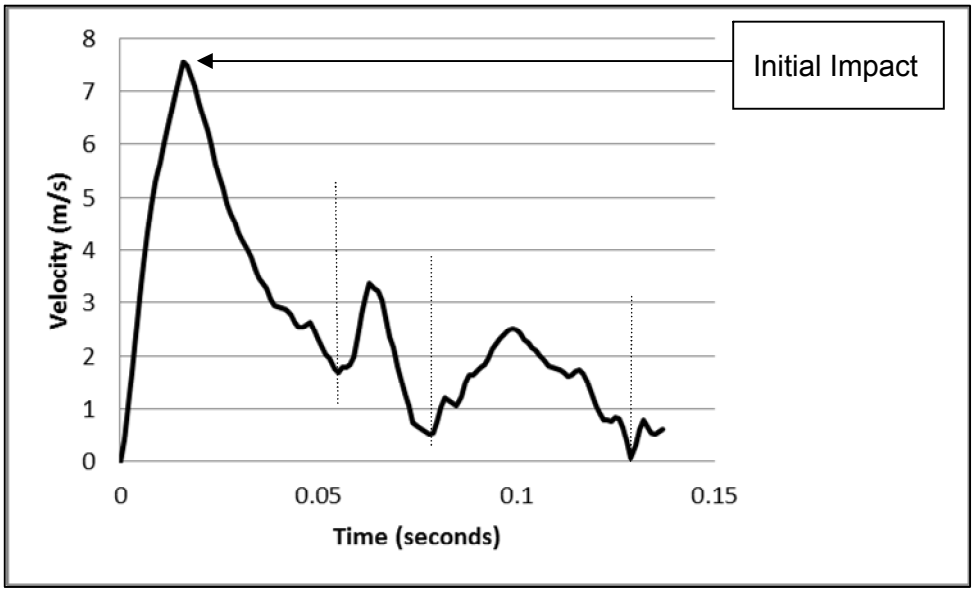

Figure 26 - The LS-DYNA® velocity versus time

The process pipe is bumping into the crush pipe. The crush pipe is also known as the bumper design; this is derived from the bumping effect that is shown in the velocity against time graph in **Figure 26**. The bumper effect will reach a negative value once the thrust of the fluid has reduced or the reservoir, which provides the fluid, has emptied and no large thrust is present.

Table 9 - Summary of dynamic hinge values

Calculation method	Value (m)
Equation (3.4)	2.2
LS-DYNA®	2.3

The dynamic hinge has now been calculated using two methods; by utilizing equation (3.4) and by utilizing LS-DYNA® software. The values are listed in **Table 9**.

4.4 Crush pipe

The energy of the process pipe is absorbed by the crush pipe. In **Figure 27** the deformation of the crush pipe can be seen. The crush pipe deforms from its original form but does not allow the process pipe to crush into the wall. The crush pipe sufficiently absorbs the process pipe's energy by entering the plastic region of the material. **Table 10** summarizes the results.

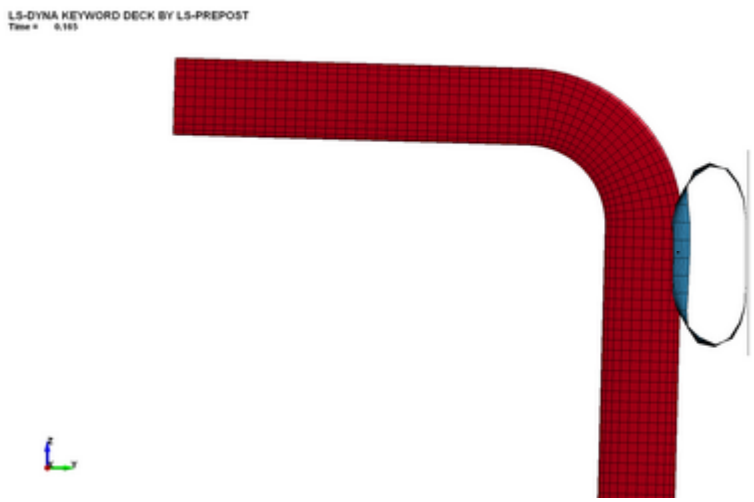

Figure 27 - Crush pipe

Table 10 - Summary of crush pipe results

Calculation method	Result (kJ)
Equation (3.22)	288.95
LS-DYNA®	275.94

4.5 Conclusion

The pre- and post-processing of the problem are critical to the final portrayal of the dynamic finite element analysis results. The non-linear elastic-plastic behavior is determined in the dynamic finite element analysis. There is a 4.5% difference between the formula of Roemer and East (1980) and the dynamic finite element analysis (Table 9). This is due to the bending that is not included in the formula. Although it is excluded the formula provides a good basic design to establish the concept of the design before a detailed analysis is performed.

The dynamic hinge position is verified by a dynamic finite element analysis and determined to be 2.30 m from the first elbow, which is within 5% of the result obtained by the first-order analysis. The finite element analysis showed no static hinge due to the presence of the crush pipe that was included in the analysis.

The crush pipe whip restraint is successful in absorbing a large amount of the dynamic energy through the deflection it undergoes. The forces transferred to the wall must not be ignored even though they are not part of this dissertation.

The dynamic finite element analysis can be used to confirm the concept prior to, or during the detail design.

Chapter 5

Conclusions and recommendations

In addition to all the safety requirements incorporated within a nuclear power plant, the influence of a pipe rupture on the environment can be severe. The regulatory commission has included the mitigation of pipe breaks, the result of which can be damaging to the integrity of the operating plant. This research focused on the analysis that is used to mitigate the effect of these events by the installation of restraints to restrict pipe motion in the event of a pipe rupture.

5.1 Summary of research results

This research project aimed to calculate the thrust forces applicable to a pipe break scenario, the resultant whipping pipe trajectory, and determining the best type of restraint to be used to restrict this motion. The literature review led to the adoption of the ANS 58.2 method (ANS, 1998) for determining the fluid thrust force. This method is based on the experiments performed by Moody (1969). In order to fulfill this, the following calculation process for the input values is used:

Thrust force:

a. The initial thrust force (78.68 kN) and the steady-state thrust force (98.34 kN) for the break is determined by applying the ANS 58.2 code criteria and calculation method (ANS, 1998).

The time-history graph of the flow based on the predictions in **Chapter 2.3.1** indicates that steady-state conditions are achieved in 0.638 s (**Chapter 3.3**).

Plastic hinge:

b. A dynamic plastic hinge will occur at 2.2 m after the first pipe elbow. The static plastic hinge will occur at 0.29 m after the first pipe elbow (**Chapter 3.4**).

The dynamic hinge of the pipe determined in **Chapter 3.4** excludes the bending of the pipe.

Pipe whip restraint geometry:

c. The calculated loads indicated in **Tables 4 and 6** are the sizing results of two different type of whip restraints: U-bar and crush pipe.

d. The best restraint for this specific application has been evaluated in the form of the Pugh matrix in **Table 7**.

For the design of the pipe whip restraint, the following functional characteristics are applicable:

e. Avoidance of excessive impact loads on existing plant structures by containing the whip of the pipe in the U-bar or by the crush pipe deformation containing the process pipe.

f. Prevention of impact damage to neighboring pipes and components critical to safe plant shutdown by containing or restricting the movement of the process pipe to the pipe whip restraint.

Assessment of the influence on the plant environment includes:

g. Avoidance of human access or interference during operation.

h. The structure must be maintenance free.

i. Design for a once-off operation.

Pipe whip restraints are required where no other reasonable engineering solution can be adopted to mitigate the pipe whip effect. The extent of the engineering solutions can be mitigated through the use of logic diagrams for pipe rupture evaluation as indicated in **Figure 2** in **Chapter 1**.

The detailed results of this research are as follows:

1. Apply a numerical design philosophy to a break using the energy method.

The U-bar and crush pipe concepts evaluated in this dissertation were both designed to accommodate the forces of the break. The energy balance method used for the conceptual design was shown to be a very useful iteration and conceptual design tool.

The energy absorbed by the crush pipe resulted in the deflection displayed in **Figure 27**.

2. Conceptually design and evaluate pipe whip restraints.

There is a 4.5% difference in value of which is due to the bending that is not included in the formula of **Chapter 3.4**. Although it is excluded the formula provides a good design to establish the concept of the design before a detailed analysis is performed.

3. Validate the pipe whip design with a dynamic finite element analysis.

The dynamic hinge position is verified by a dynamic finite element analysis and determined to be 2.30 m from the first elbow, which is within 5% of the result obtained by the first-order analysis. The finite element analysis showed no static hinge due to the presence of the crush pipe that was included in the analysis. The importance of the validation finite element analysis is to physically validate that no secondary hinge will form and that the dynamic hinge is forming at the same location as calculation by equation (3.4).

The crush pipe size is established by the energy method in equation (3.22). The strain energy must be less than the potential energy for the crush pipe to be successful. During the validation of the pipe break the crush pipe is successful in retaining the energy. This is due to it not collapsing during the dynamic finite element analysis. Further work on the crush pipe must be performed during the detail design of the crush pipe. A method from the dynamic finite element analysis to a static finite element analysis is a possible route to investigate.

The pipe break analysis scenario analyzed herein assumed a guillotine break at a terminal end, as defined in ANS 58.2 (ANS, 1998). The pipe can result in damage to essential structures or components, considering any safety related components near the pipe rupture.

Further study in the field of crack growth combined with pipe break will be of advantage to future plant owners and utility engineers both in nuclear and petrochemical areas.

The pipe rupture can be applied to any geometry or layout of a piping system. This geometrical or layout features can be an area of future study.

5.2 Conclusion

The ANS 58.2 method (ANS, 1998) is standard practice for a nuclear power plant and it is adopted by most engineering companies worldwide. Further research indicated that the method following the determination of thrust differs from case to case.

It is the author's opinion that the fluid stream jet may result in additional jet forces on the piping system and pipe whip restraint structure. Further analysis is required to evaluate the jet force geometry and determine whether the fluid will have an additional force on the problem presented.

In the example used the jet geometry does not have an effect on the pipe whip structure and no additional jet forces are included in the calculation.

Due to the large difference in deflection more work needs to be performed on the deflection calculation in future, but the crush pipe was successful in absorbing the energy.

The plant environment and the supporting structures are the determining factors of which the type of pipe whip restraint is chosen to be considered. The U-bar requires a large structure with at least three overlay plates to the wall, while the crush pipe requires only one overlay plate and a small backup structure. The crush pipe restraint is therefore preferable to the U-bar but it is not always practical to install for a whip away from a wall.

The plant model and three-dimensional environment assist with the functional characteristics of the pipe whip restraint and the influence the break will have on the rest of the plant environment.

In the non-nuclear environment a pipe whip restraint can be used after a risk based inspection (on any type of plant) has been concluded. Additional precaution is required. In Chapter 1 the preventative measures at the plants could have protected the personnel at the plants during the pipe break that occurred.

The pipe whip restraint will not influence or keep the pipe from breaking; it will only restrain the dynamic forces to a safe level for the rest of the plant to have a safe shutdown and to protect the personnel on the plant from any dynamic forces resulting in fatal injuries.

5.3 Recommendations

Further work on this topic is needed in the detail design of pipe whip restraints. The empirical method must be verified by an experiment on a specific type of design. Once this has been successfully done the same test article must be verified by the energy balance method.

The finite element analysis method, the practical test, the empirical method and the energy balance method has to be compared and verified for each type of design.

The analysis code needs to be verified and validated for use in nuclear applications. This can only be achieved with experimental and other type of calculation methods.

A sensitivity analysis should be performed on the time to reach the steady state thrust. This time period should be divided into several scenarios and combinations of different time periods.

The method can be applied to other pipe break locations, for example not at terminal ends. The LS-DYNA® analysis can be repeated/performed for a U-bar pipe whip restraint to illustrate the relative performance between this design and the crush pipe design.

Further investigation is required in the field of risk analysis based inspection on non-nuclear plants. When a pipe has been identified as a potential break risk the pipe whip restraint can be installed as a safety device to protect the plant and its personnel. During this timeframe a new pipe system can be designed and manufactured. This will ensure the plant and its personnel will be safe from any hazards resulting from a pipe break, namely whipping pipe creating debris that get airborne and damage control rooms, offices or other equipment on-site.

References

American National Standards Institute (ANSI), 1994. *ANSI N690 Specification for Safety-Related Steel Structures for Nuclear Facilities.* Illinois: American Nuclear Society.

American Nuclear Society (ANS), 1998. *ANSI/ANS-58.2 Design Basis for protection of light water nuclear power plants against the effects of postulated pipe rupture.* Illinois: American Nuclear Society.

Andersen, A., Bergmann, H. and Hortsmann, R., 2001. Protection against high-energy line breaks in WWER power plants. *Nuclear Engineering and Design,* 206 (2-3), pp.119-128.

ASME, 2004a: American Society of Mechanical Engineers, 2004. *ASME boiler and pressure vessel code section II: Properties (customary materials)*. New York: The American Society of Mechanical Engineers.

ASME, 2004b: American Society of Mechanical Engineers, 2004. *ASME boiler and pressure vessel code section III: Rules for construction of nuclear facility components.* New York: The American Society of Mechanical Engineers.

ASME, 2004c: American Society of Mechanical Engineers, 2004. *ASME boiler and pressure vessel code section V: Non-destructive examination.* New York: The American Society of Mechanical Engineers.

ASME, 2004d: American Society of Mechanical Engineers, 2004. *ASME boiler and pressure vessel code section XI: Rules for inservice inspection of nuclear power plant components.* New York: The American Society of Mechanical Engineers.

ASME, 2004e: American Society of Mechanical Engineers, 2004. *ASME boiler and pressure vessel code* B31.10*: Power piping.* New York: The American Society of Mechanical Engineers.

ASME, 2004f: American Society of Mechanical Engineers, 2004. *ASME boiler and pressure vessel code* B36.10*: Welded and seamless wrought steel pipe.* New York: The American Society of Mechanical Engineers.

ASME, 2009: American Society of Mechanical Engineers, 2009. *International Steam Tables for Industrial Use*. 2nd ed. New York: The American Society of Mechanical Engineers.

Barna, I. F., and Ezsöl, G., 2011. Multiple condensation induced water hammer events, experiments and theoretical investigations. *Kerntechnik*, 76 (4), pp. 231-236.

Birkhoff, G. and Zarantonello, E.H.,1957. Jets, wakes and cavities. New York: Academic Press.

Bisconti, N., Lazzeri, L. and Strona, P.P., 1976. Pipe whip analysis for nuclear reactor applications. *Nuclear Engineering and Design,* 37 (3), pp. 347-360.

Boresi, A.P. and Schmidt, R.J., 2003. *Advanced mechanics of materials*. 6th ed. Danvers, MA: John Wiley.

Calonius, K., 2009. *Numerical studies of behavior of pipelines (VTT-R-01025-09)*. Laskut: Technical Research Centre of Finland.

Calonius, K., 2010. *Numerical studies of behavior of pipelines, Part 2 (VTT-R-01214-10)*. Laskut: Technical Research Centre of Finland.

Charalambus, B. and Labes, M., 1993. Structural integrity of whipping pipes following a postulated circumferential break – a contribution to determining strain levels under faulted conditions. *Nuclear Engineering and Design,* 144 (1), pp. 91-99.

Corrosion Doctors, 2011. *Nuclear accident 1*. [online] Available at: <http://www.corrosion-doctors.org/NuclearIndustry/nuclear-accident-1.htm> [Accessed 13 July 2012].

Enis, R.O., Bernal, D.B. and Burdette, E.G., 1980. *A design guide for evaluation of barriers for impact from whipping pipes*. Knoxville, TN: ASCE.

Fauske, H.K., 1962. *Contribution to the theory of two-phase, one component critical flow* (*ANL-6633).* Illinois: Argonne National Laboratory.

Fauske, H.K., 1965. The discharge of saturated water through tubes. *American Institute of Chemical Engineers Chemical Engineering Symposium series*, 61 (59).

Gieck, K. and Gieck, R., 1996. *A collection of technical formulae*, D-82110. Translated from German by J. Walters. Germany: Germering.

Hearn, E.J., 2000. *An introduction to the mechanics of elastic and plastic deformation of solids and structural materials*. 3rd ed. Oxford: Butterworth-Heinemann.

Henry, R.E., 1970. *An experimental study of Low-quality steam-water critical flow at moderate pressure (ANL-7740)*. Illinois: Argonne National Laboratory.

Henry, R.E. and Fauske, H.K., 1971. The two phase critical flow of one-component mixtures in nozzle and short tubes. *ASME Journal of Heat Transfer*, 93 (2), pp. 179-187.

Inman, D.J., 2009. *Engineering vibrations*. 3rd ed. Upper Saddle River, NJ: Pearson Education.

Koh, S. and Lee, Y-S., 1993. Comparative study of computational model for pipe whip analysis. *International conference on structural mechanics in reactor technology.* Stuttgart, Germany. 15-20 August 1993. Amsterdam: Elsevier, pp. 85-90.

Lee, Y-S. and Koh, S., 1995. A study on the transient analysis of pipe and restraint due to impact loading. *International conference on structural mechanics in reactor technology*. Brazil, 13-18 August 1995. Porto Alegre: Universidade Federal do Rio Grande do Sul.

Livermore Software Technology Corporation (LSTC), 2009. *LS-DYNA®.* [online] Available at: < http://www.lstc.com/products/ls-dyna> [Accessed 15 August 2011].

Ma, S.M. and Bathe, K.J., 1976. On finite element analysis of pipe whip problems. *Nuclear Engineering and Design,* 37(3), pp.413-429.

Micheli, I. and Zanaboni, P., 2003. An analytical validation of simplified methods for the assessment of pipe whip characteristics. *International conference on structural mechanics in reactor technology*. Prague, Czech Republic. 17–22 August 2003.

Milne-Thompson, L. M., 1963. *Theoretical hydrodynamics*. 4th ed. New York: The Macmillan Company.

Miyazaki, N. et al., 1983. Experimental and analytical studies of four-inch pipe whip tests under PWR LOCA conditions. *International Journal of Pressure Vessels and piping,* 15 (2), pp. 125-150.

Moody, F.J., 1965. Maximum two-phase vessel blowdown from pipes. *ASME Journal of Heat Transfer*, 88 (3).

Moody, F.J., 1969. Prediction of blowdown thrust and jet forces. *ASME-AIChE heat transfer conference*. Minneapolis, Minnesota. 3-6 August 1969. New York: American Society of Mechanical Engineers.

Morisaki, S., 2008. *Risk based inspection*. Graduate School of Information. Science, Nara Institute of Science and Technology, Japan.

Parametric Technology Corporation® (PTC), 2007. *Mathcad-engineering Calculations Software*. Computer software. Needham, Massachusetts.

Patel, J.R., 2005. Risk based inspection. *Middle East Nondestructive Testing Conference and Exhibition*. Bahrain, Manama. 27-30 November 2005.

Peach, J.M., et al., 1977. Local crush rigidity of pipes and elbows. *International conference on structural mechanics in reactor technology*. San Francisco, California. 15-19 August 1977, pp. F3/8.

PennEnergy, 2011. Survey of Leak-Before-Break in Nuclear Plant Piping. [online] Available at: < http://www.pennenergy.com/pennenergy-2/en-us/index/articles/pe-article-tools-template.articles.nuclear-power-international.volume3.issue1.nucleus.An_Historical_Survey_of_Leak-Before-Break_in_Nuclear_Plant_Piping.html > [Accessed 25 July 2012].

Pugh, S., 1981. Concept selection: A method that works. Hubka, V. (ed.), Review of design methodology. *Proceedings international conference on engineering design*. Rome. March 1981. Heurista, pp. 497-506.

Reid, S.R., Wang, B. and Aleyaasin, M., 2011. Structural modeling and testing of failed high energy pipe runs: 2D and 3D pipe whip. *International Journal of Pressure Vessels and Piping*, vil. 88, no. 5-7, pp. 189-197.

Roemer, R.E. and East, G.H., 1980. Prediction of large deformation pipe whip and barrier impact: a simplified approach. *Pressure vessel and piping conference*. San Francisco, California. 12-15 August 1980. New York: American Society of Mechanical Engineers.

South Africa, 1993. Occupational Health and Safety Act No. 85 of 1993. Pretoria: Government Printing Works.

Spada, A.J. and Goldstein, N.A., 1980. Efficient pipe whip restraint design. *Pressure vessel and piping conference*. San Francisco, California. 12–15 August 1980. New York: American Society of Mechanical Engineers.

United States Nuclear Regulatory Commission (USNRC), 1982. *NUREG/CR-2426RM Design charts for nonlinear systems with gapped supports under impulse loads*. Pittsburgh, PA: The Government Printing Office.

United States Nuclear Regulatory Commission (USNRC), 1985. Information notice no. *IN 85–05: Pipe whip restraints*.

United States Nuclear Regulatory Commission (USNRC), 2005. *Code of Federal Regulations (CFR) 10 CFR 50 Domestic licensing of production and utilization facilities*. Pittsburgh, PA: The Government Printing Office.

Vongmongkol, S., Faal-Amiri, A. and Srivastava, H.M., 2011. Determination of pipe whip restraint location to prevent plastic hinge formation in high energy piping systems. Pressure *vessel and piping conference*. Baltimore, Maryland 17–21 July 2011. New York: American Society of Mechanical Engineers.

Voros, G., Zsidi, Z., and Vigh, Z., 2002. Analysis of the effects of postulated pipe rupture. *3rd Conference on mechanical engineering Gépészet 2002*. Budapest, Hungary. 30-31 May 2002.

Weigand, G.G., Thompson, S.L. and Tomasko, D., 1983. *Two phase jet loads*. National Technical Information Service. Springfield, VA: National Government Publication.

Welding Research Council (WRC), 1987. Bulletin 321, *The dynamic deformation of piping*. New York: Welding Research Council.

Wikipedia, 2011. *Stuart Pugh*. [online] Available at: <http://en.wikipedia.org/w/index .php? title=Stuart_Pugh&oldid=438647958> [Accessed 25 March 2011].

Wikipedia, 2012. *Mohave Power Station*. [online] Available at: < http://en.wikipedia.org/wiki/ Mohave_Power_Station> [Accessed 13 July 2012].

Yang, J.L., Lu, G.Y., Yu, T.X. and Reid, S.R., 2009. Experimental study and numerical simulation of pipe-on-pipe impact. *International Journal of Impact Engineering*, vol. 36, no. 10-11, pp. 1259-1268.

Young, N., 2010. Ceremony observes 25th anniversary of tragedy at Mohave Generating Station. *The Laughlin Nevada Times*, [online] (Last updated 2.05 on 14th June 2010) Available at: <http://www.laughlintimes.com/articles/2010/06/16/news/local/news998.txt> [Accessed on 2 November 2012]

Appendix A

Thrust force calculation

[adapted from Parametric Technology Corporation® (PTC) Mathcad file]

Nomenclature (PTC, 2007)

A_a	Jet area at the asymptotic plane	(m^2)	(ANS, 1998)
A_e	Break plane area	(m^2)	(ANS, 1998)
A_R	Asymptotic area ratio	(dimensionless)	(ANS, 1998)
A_{ZOI}	Zone of influence area	(m^2)	(ANS, 1998)
C_T	Steady-state thrust coefficient	(dimensionless)	(ANS, 1998)
C_{Te}	Steady-state thrust coefficient	(dimensionless)	(ANS, 1998)
D_a	Jet diameter at the asymptotic plane	(m)	(ANS, 1998)
D_c	Jet core diameter	(m)	(ANS, 1998)
D_e	Pipe inside diameter	(m)	(ANS, 1998)
D_{nozzle}	Nozzle inside diameter	(m)	
D_O	Pipe outside diameter	(m)	(ASME, 2004f)
D_{ZOI}	Zone of influence diameter	(m)	
h_o	Fluid enthalpy at the initial conditions	(J/kg)	
h_{sat}	Saturated enthalpy at the initial conditions	(J/kg)	
L	Distance from break plane to target	(m)	(ANS, 1998)
L_a	Break plane to asymptotic distance plane	(m)	(ANS, 1998)
L_c	Core length	(m)	(ANS, 1998)
L_{ZOI}	Zone of influence length	(m)	
P_{amb}	Ambient pressure taken as one atmosphere	(kPa)	
P_o	Initial pressure in the source	(kPa)	(ANS, 1998)
r_i	Pipe inside radius	(m)	(ASME, 2004f)
r_o	Pipe outside radius	(m)	(ASME, 2004f)
t	Pipe wall thickness	(m)	(ASME, 2004f)
T_{INT}	Initial thrust force	(kN)	(ANS, 1998)
T_{sat}	Saturation temperature at PO	(°C)	
T_{SS}	Steady-state thrust force	(kN)	(ANS, 1998)
T_{sub}	Jet sub-cooling stagnation condition	(K)	(ANS, 1998)
T_o	Initial temperature in the source	(°C)	
ρ_o	Fluid density at the initial conditions	(kg/m^3)	

List of equations

Asymptotic area ratio:

$$A_R(A_a, A_e) := \frac{A_a}{A_e} \tag{A1}$$

Break plane to asymptotic plane distance:

$$L_a(A_a, A_e, D_e) := \frac{1}{2}\cdot\left(\sqrt{\frac{A_a}{A_e}} - 1\right)\cdot D_e \tag{A2}$$

Break plane area:

$$A_e(D_e) := \pi\cdot\frac{D_e^{\,2}}{4} \tag{A3}$$

Core length of jet region 1:

$$L_c(\Delta T_{sub}, D_e) := \left(0.26\cdot\frac{\sqrt{\Delta T_{sub}}}{\sqrt{1K}} + 0.5\right)\cdot D_e \tag{A4}$$

Initial thrust force:

$$T_{INT}(P_o, A_e) := P_o\cdot A_e \tag{A5}$$

Jet core diameter of region 1:

$$D_c(C_{Te}, L, L_c, D_e) := \sqrt{C_{Te}}\cdot\left(1 - \frac{L}{L_c}\right)\cdot D_e \tag{A6}$$

Jet diameter of asymptotic plane:

$$D_a(A_a) := \sqrt{\frac{4\cdot A_a}{\pi}} \tag{A7}$$

Steady-state thrust force:

$$T_{ss}(C_T, P_o, A_e) := C_T\cdot P_o\cdot A_e \tag{A8}$$

Zone of influence area:

$$A_{ZOI}(L_{ZOI}, L_a, D_a, A_a) := \left[1 + \frac{2\cdot(L_{ZOI} - L_a)}{D_a}\cdot\tan(10\,\text{deg})\right]^2 \cdot A_a \qquad \text{(A9)}$$

Zone of influence diameter:

$$D_{ZOI}(A_{ZOI}) := \sqrt{\frac{4\cdot A_{ZOI}}{\pi}} \qquad \text{(A10)}$$

Zone of influence length:

$$L_{ZOI}(D_e) := 10\cdot D_e \qquad \text{(A11)}$$

Pipe inside diameter:

$$D_e(D_{nozzle}) := D_{nozzle} \qquad \text{(A12)}$$

Pipe outside diameter:

$$D_o(D_e, t) := D_e + 2\cdot t \qquad \text{(A13)}$$

Pipe inside radius:

$$r_i(D_e) := \frac{D_e}{2} \qquad \text{(A14)}$$

Pipe outside radius:

$$r_o(D_o) := \frac{D_o}{2} \qquad \text{(A15)}$$

A.1 Fluid conditions

The break occurs at the terminal end specified in **Chapter 2**. The following fluid conditions are used for this calculation.

Fluid conditions:

$P_o := 5.771\ MPa$	(Chapter 2)
$T_o := 273.06\ °C$	(Chapter 2)
$P_{amb} := 0.101\ MPa$	(Ambient pressure)
$T_{sat} := T_o$	(ASME, 2009)
$\rho_o := 762.665\ \frac{kg}{m^3}$	(ASME, 2009)
$h_o := 1.20 \cdot 10^6\ \frac{J}{kg}$	(ASME, 2009)
$h_{sat} := h_o$	(ASME, 2009)

State of the fluid: saturated liquid

A.2 Pipe dimensions

Pipe is 150NB, schedule 160 (ASME, 2004f)

The pipe variables are visually indicated in **Figure A.1**.

$D_{nozzle} := 131.75\ mm$ (ASME, 2004f)

$t := 18.26\ mm$ (ASME, 2004f)

From equation A12:

$D_e(D_{nozzle}) = 131.75\ \cdot mm$

From equation A13:

$D_o(D_e(D_{nozzle}), t) = 168.27\ \cdot mm$

From equation A14:

$r_i(D_e(D_{nozzle})) = 65.88\ \cdot mm$

From equation A15:

$r_o(D_o(D_e(D_{nozzle}), t)) = 84.14\ \cdot mm$

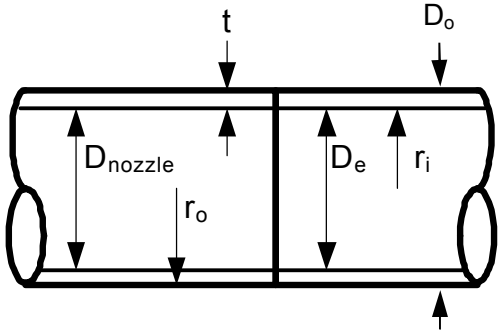

Figure A.1 - Nozzle and pipe dimensions

A.4 Initial fluid thrust force

Initial fluid thrust forces

The area of the break plane, A_e, is:

Applying equation A3:

$A_e(D_e(D_{nozzle})) = 0.01 \cdot m^2$

The initial thrust force, T_{INT}, is by applying equation A5:

$T_{INT}(P_o, A_e(D_e(D_{nozzle}))) = 78.68 \cdot kN$

A.5 Steady-state thrust force

The pressure vessel forms the reservoir for the break. The break forms at the nozzle and can be considered frictionless flow. The steady-state thrust coefficient for saturated, frictionless flow:

$C_T := 1.25$

Applying equation A8:

$T_{ss}(C_T, P_o, A_e(D_e(D_{nozzle}))) = 98.34 \cdot kN$

A.6 Jet-spray geometry

The break is a circumferential break with full separation. The jet geometry given below is calculated using ANS 58.2 (1998), Appendix C.
The expanding jet model is modeled after ANS 58.2 (ANS, 1998), Appendix C, **Figure C-1** (A) and is visually represented in **Figure A.2**:

A.6.1 Region 1 ($0 \le L \le L_c$)

Break plane fluid conditions:

$\Delta T_{sub} := T_{sat} - T_o$ Sub-cooling at the break plane

$\Delta T_{sub} = 0\,K$

$C_{Te} := 1.26$

The steady-state thrust coefficient for saturated, frictionless flow is determined from ANS 58.2 (ANS, 1998), Fig B-5.

Jet core length:

Applying equation A4:

$L_c(\Delta T_{sub}, D_e(D_{nozzle})) = 65.88 \cdot mm$

The jet core diameter at the break plane:

$L := 0ft = 0 \cdot m$

Applying equation A6:

$D_c(C_{Te}, L, L_c(\Delta T_{sub}, D_e(D_{nozzle})), D_e(D_{nozzle})) = 147.89 \cdot mm$

A.6.2 Region 2 ($L_c < L < L_a$):

Asymptotic Area (A_a) by applying equation A1:

$A_a/A_e = 43.85$

$A_a := 43.85 \cdot A_e(D_e(D_{nozzle}))$

$A_a = 0.6 \cdot m^2$

The distance from the break plane to the asymptotic plane by applying equation A2:

$L_a(A_a, A_e(D_e(D_{nozzle})), D_e(D_{nozzle})) = 370.34 \cdot mm$

The diameter is from equation A7:

$D_a(A_a) = 872.44 \cdot mm$

A.6.3 Region 3 ($L \geq L_c$):

Applying equation A11:

$L_{ZOI}(D_e(D_{nozzle})) = 1317.5 \cdot mm$

Applying equation A9:

$A_{ZOI}(L_{ZOI}(D_e(D_{nozzle})), L_a(A_a, A_e(D_e(D_{nozzle})), D_e(D_{nozzle})), D_a(A_a), A_a) = 1.14 \cdot m^2$

Applying equation A10:

$D_{ZOI}(A_{ZOI}(L_{ZOI}(D_e(D_{nozzle})), L_a(A_a, A_e(D_e(D_{nozzle})), D_e(D_{nozzle})), D_a(A_a), A_a)) = 1206.46 \cdot mm$

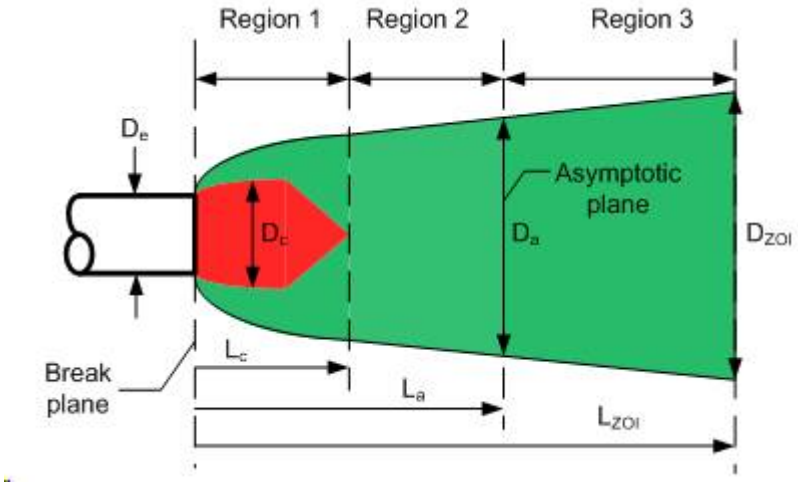

Figure A.2 - The expanding fluid jet geometry for a circumferential break with full separation

Appendix B

Hinge calculation
(extracted from PTC Mathcad file)

Nomenclature (PTC, 2007)

A_{metal}	Pipe metal area	(m^2)	(Gieck and Gieck, 1996)
A_{pipe}	Pipe fluid area	(m^2)	(Gieck and Gieck, 1996)
c_o	Sonic velocity	(m/s)	
D_i	Pipe inside diameter	(m^2)	(Gieck and Gieck, 1996)
DLF	Dynamic load factor	(dimensionless)	
D_{nozzle}	Nozzle inside diameter	(m)	
D_O	Pipe outside diameter	(m)	(ASME, 2004f)
d_x	Length of change in the X direction	(m)	
d_y	Length of change in the Y direction	(m)	
d_z	Length of change in the Z direction	(m)	
g_c	Gravitational constant	(m/s^2)	
$L_{DynamicHinge}$	Length of the dynamic hinge programmed	(m)	
L_m	Length of pipe to the first elbow	(m)	
L_{pipe}	Length of pipe from break to reservoir	(m)	
M_{el}	Total point mass	(kg)	(Roemer and East, 1980)
M_p	Plastic moment	(kN.m)	(Roemer and East, 1980)
$M_{Plastic}$	Plastic moment programmed	(kN.m)	
m_{ins}	Point mass of insulation	(kg)	
m_{liquid}	Point mass of liquid	(kg)	
m_{pipe}	Mass of length pipe	(kg)	
m_p	Point mass of pipe	(kg)	
m_{valve}	Point mass of valve	(kg)	
P_o	Operating pressure	(kPa)	
r_i	Pipe inside radius	(m)	(ASME, 2004f)

r_o	Pipe outside radius	(m)	(ASME, 2004f)
S_y	Metal yield stress	(kPa)	(ASME, 2004a)
S_{YD}	Metal yield design stress	(kPa)	(ANS, 1998)
t	Pipe wall thickness	(m)	(ASME, 2004f)
T	Thrust	(kN)	
t_{dep}	Time to depressurization	(m)	
T_{INT}	Initial thrust force	(kN)	(ANS, 1998)
T_{DYN}	Dynamic thrust	(kN)	
t_{ss}	Time to reach steady-state	(m)	
T_{SS}	Steady-state thrust force	(kN)	(ANS, 1998)
η_{ins}	Insulation mass per unit length	(kg/m)	
η_{pipe}	Pipe mass per unit length	(kg/m)	
ρ_{metal}	Pipe metal density	(kg/m^3)	(ASME, 2004a)
ρ_o	Fluid density at the initial conditions	(kg/m^3)	

List of equations

Plastic bending moment:

$$M_{Plastic}(r_i, r_o, S_{YD}) := \frac{4}{3} \cdot S_{YD} \cdot \left(r_o^{\,3} - r_i^{\,3} \right) \tag{B1}$$

Pipe metal area:

$$A_{metal}(D_o, D_i) := \pi \left(\frac{D_o^{\,2}}{4} - \frac{D_i^{\,2}}{4} \right) \tag{B2}$$

Pipe fluid area:

$$A_{pipe}(D_i) := \pi \left(\frac{D_i^{\,2}}{4} \right) \tag{B3}$$

Mass per length:

$$\eta_{pipe}(A_{metal}, \rho_{metal}) := A_{metal} \cdot \rho_{metal} \tag{B4}$$

Effective mass of pipe:

$$m_{pipe}(\eta_{pipe}, L_m) := \eta_{pipe} \cdot L_m \tag{B5}$$

Effective mass of liquid:

$$m_{liquid}(A_{pipe}, L_m, \rho_o) := A_{pipe} \cdot L_m \cdot \rho_o \tag{B6}$$

Pipe inside radius:

$$r_i(D_i) := \frac{D_i}{2} \tag{B7}$$

Pipe outside radius:

$$r_o(D_o) := \frac{D_o}{2} \tag{B8}$$

Pipe inside diameter:

$$D_i(D_{nozzle}) := D_{nozzle} \tag{B9}$$

Pipe outside diameter:

$$D_o(D_i, t) := D_i + 2 \cdot t \tag{B10}$$

$$L_{DynamicHinge}\left(D_i, D_o, L_m, M_P, m_{valve}, \eta_{ins}, \rho_{metal}, \rho_o, T\right) := \left| \begin{array}{l} A_{metal} \leftarrow \pi\left(\frac{D_o^{\,2}}{4} - \frac{D_i^{\,2}}{4}\right) \\ A_{pipe} \leftarrow \pi\left(\frac{D_i^{\,2}}{4}\right) \\ \eta_{pipe} \leftarrow A_{metal} \cdot \rho_{metal} \\ m_{pipe} \leftarrow \eta_{pipe} \cdot L_m \\ m_{liquid} \leftarrow A_{pipe} \cdot L_m \cdot \rho_o \\ m_{ins} \leftarrow \eta_{ins} \cdot L_m \\ M_{el} \leftarrow m_{pipe} + m_{liquid} + m_{ins} + m_{valve} \\ m_p \leftarrow \eta_{pipe} + \eta_{ins} + \rho_o \cdot A_{pipe} \\ \frac{-\left(-3 \cdot M_P\right) + \left[\left(-3 \cdot M_P\right)^2 - 4 \cdot (T) \cdot \left(-6 \cdot M_P\right) \cdot \left(\frac{M_{el}}{m_p}\right)\right]^{0.5}}{2 \cdot T} \end{array} \right. \tag{B11}$$

Hinge coordination:

$$HingeCoord := BreakCoord + \begin{pmatrix} dx \\ dy \\ dz \end{pmatrix} \tag{B12}$$

Radius of hinge:

$$Radius := BreakCoord - HingeCoord \tag{B13}$$

Time to reach steady-state thrust force:

$$t_{ss} := 2 \cdot L_{pipe} \cdot \sqrt{\frac{\rho_o}{2 \cdot g_c \cdot P_o}} \tag{B14}$$

B.2 Calculation data

The following values are used for this calculation:

$T_{INT} := 78.68\ kN$ (Appendix A)

$T_{SS} := 98.34\ kN$ (Appendix A)

$DLF := 2$ (ANS, 1998)

Fluid Conditions:

$\rho_o := 762.67\ \frac{kg}{m^3}$ (ASME, 2009)

$\rho_{metal} := 7855.81\ \frac{kg}{m^3}$ (ASME, 2004a)

$\eta_{ins} := 13.1\ \frac{kg}{m}$

$S_y := 1.73 \cdot 10^5 kPa$ (ASME, 2004a)

10% increase due to the dynamic effect described in ANS 58.2 (ANS, 1998):

$S_{YD} := 1.1 \cdot S_y$ (ANS, 1998)

$P_o := 5.771\ MPa$ (Appendix A)

B.3 Pipe dimensions:

Pipe is 150NB, schedule 160. (ASME, 2004f)

Material specified in **Chapter 2** is SA-333, Grade 6.

The pipe variables are visually indicated in **Figure A.1**.

$D_{nozzle} := 131.75\ mm$

$t := 18.26\ mm$

Applying equation B9:

$D_i(D_{nozzle}) = 131.75\ \cdot mm$

Applying equation B10:

$D_o(D_i(D_{nozzle}), t) = 168.27\ \cdot mm$

Applying equation B7:

$r_i(D_i(D_{nozzle})) = 65.88\ \cdot mm$

Applying equation B8:

$r_o(D_o(D_i(D_{nozzle}), t)) = 84.14\ \cdot mm$

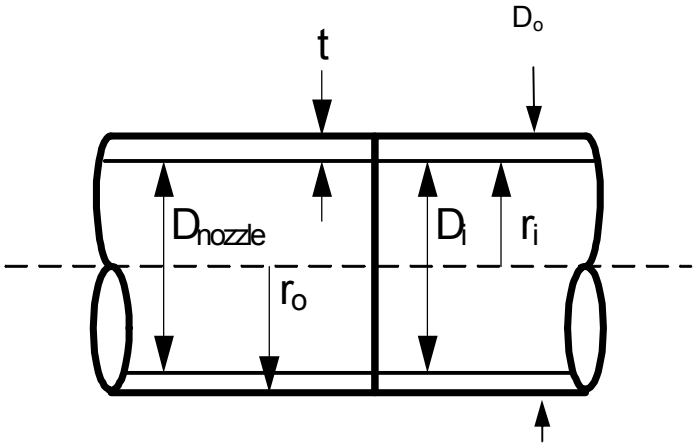

Figure B.1 - Nozzle and pipe dimensions

B.4 Pipe length before elbow:

Figure B.2 illustrates that the pipe length up to the first bend will be modeled in the calculation as a simple mass (Roemer and East, 1980).

Applying equation B2:

$$A_{metal}\left(D_o\left(D_i\left(D_{nozzle}\right),t\right),D_i\left(D_{nozzle}\right)\right) = 0.01\cdot m^2$$

Applying equation B3:

$$A_{pipe}\left(D_i\left(D_{nozzle}\right)\right) = 0.01\cdot m^2$$

Applying equation B4:

$$\eta_{pipe}\left(A_{metal}\left(D_o\left(D_i\left(D_{nozzle}\right),t\right),D_i\left(D_{nozzle}\right)\right),\rho_{metal}\right) = 67.6\cdot\frac{kg}{m}$$

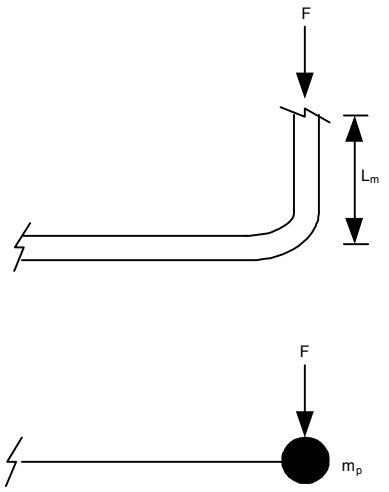

Figure B.2 - Visualization of pipe being modeled as a point mass

B.5 Plastic Bending, M_P for straight pipe:

Applying equation B1:

$$M_P := M_{Plastic}\left(r_i\left(D_i\left(D_{nozzle}\right)\right),r_o\left(D_o\left(D_i\left(D_{nozzle}\right),t\right)\right),S_{YD}\right) = 78.581\cdot kN\cdot m$$

B.6 Hinge length determination

$L_m := 921\cdot mm$ Length of upstream pipe to the first elbow

$m_{valve} := 0\cdot lb$ No valve in this line

$T_{DYN} := DLF\cdot T_{SS}$ Dynamic trust

Applying equation B11:

$$L_{DynamicHinge}\left(D_i\left(D_{nozzle}\right),D_o\left(D_i\left(D_{nozzle}\right),t\right),L_m,M_P,m_{valve},\eta_{ins},\rho_{metal},\rho_o,T_{DYN}\right) = 2.2\cdot m$$

The deltas between the break coordinates and hinge location, dx, dy and dz, can be determined from the break coordinates:

$$\text{BreakCoord} := \begin{pmatrix} 0 \\ 0 \\ 0 \end{pmatrix} \cdot \text{m}$$

$$\text{dx} := 921 \cdot \text{mm}$$

$$\text{dy} := 0\,\text{mm}$$

$$\text{dz} := -L_{DynamicHinge}\left(D_i\left(D_{nozzle}\right), D_o\left(D_i\left(D_{nozzle}\right), t\right), L_m, M_P, m_{valve}, \eta_{ins}, \rho_{metal}, \rho_o, T_{DYN}\right)$$

$$\text{HingeCoord} := \text{BreakCoord} + \begin{pmatrix} \text{dx} \\ \text{dy} \\ \text{dz} \end{pmatrix} \tag{B12}$$

$$\text{HingeCoord} = \begin{pmatrix} 0.921 \\ 0 \\ -2.202 \end{pmatrix} \cdot \text{m}$$

The radius of rotation and the unit vector of the axis of rotation are as follows (rotation about the axis with respect to the right-hand-rule)

$$\text{Radius} := \text{BreakCoord} - \text{HingeCoord}$$

$$\left|\text{Radius}\right| = 2.386 \cdot \text{m} \tag{B13}$$

The break location, hinge location and rotational moment are shown in **Figure B.5**. In this case the pipe will rotate about the hinge location through 180° angle before hitting itself and stopping.

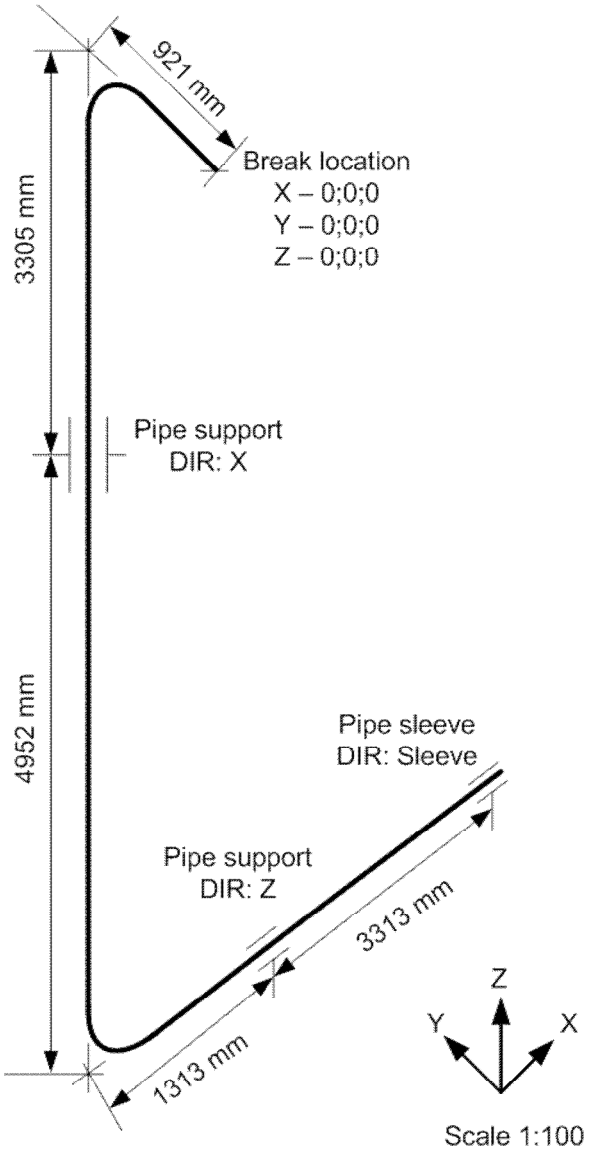

Figure B.3 - Break pipe whip motion sketch

B.7 Thrust force duration

The thrust force transient occurs while the upstream pipe depressurizes. The length of time for the upstream pipe to depressurize is estimated by taking the sonic velocity in the pipe and the length of the pipe.

$c_o := 1372 \frac{m}{s}$ Sonic velocity in cold water, ANS 58.2 (ANS, 1998)

$L_{pipe} := 39.239\ m$

$t_{dep} := \frac{L_{pipe}}{c_o} = 28.6 \cdot ms$

The time to depressurize the pipe is greater than the break opening time of 1 ms (ANS, 1998), therefore it can be assumed that the pipe will whip. The time to reach steady state can be estimated from ANS 58.2 (ANS, 1998), Appendix B, Section B.3, Paragraph (a), for non-flashing liquid.

$g_c := 32.17 \frac{ft \cdot lbm}{lbf \cdot sec^2}$ Gravitational Constant

$t_{ss} := 2 \cdot L_{pipe} \cdot \sqrt{\frac{\rho_o}{2 \cdot g_c \cdot P_o}} = 0.638\ s$ (B14)

Thrust force transient:

$0 \le time \le 1e\text{-}3\ sec$ $t_2 := 0 \cdot sec\ , 0.01\ sec\ ..\ 1 \cdot sec$

$t_1 := 0 \cdot sec\ , .001\ sec\ ..\ 0.01 \cdot sec$

$Thrust = \frac{Thrust_{init}}{1 \cdot 10^{-3} \cdot sec} \cdot time$

$1e\text{-}3\ sec < time \le t_{D\_ss}$

$Thrust(t) := \Phi\left(1 \cdot 10^{-3} sec - t\right) \cdot \left(\frac{T_{INT}}{1 \cdot 10^{-3} \cdot sec} \cdot t\right) + \Phi\left(t - 1 \cdot 10^{-3} sec\right) \cdot T_{INT} \ldots + \Phi\left(t - t_{ss}\right) \cdot \left(T_{SS} - T_{INT}\right)$

$Thrust = Thrust_{init}$

$time > t_{ss}$

$Thrust = Thrust_{ss}$

Figure B.4 and **Figure B.5** are meant to display the nature of the time function of the thrust force. As such the time scale of the figures shows the step changes, and is not meant to indicate duration of the event.

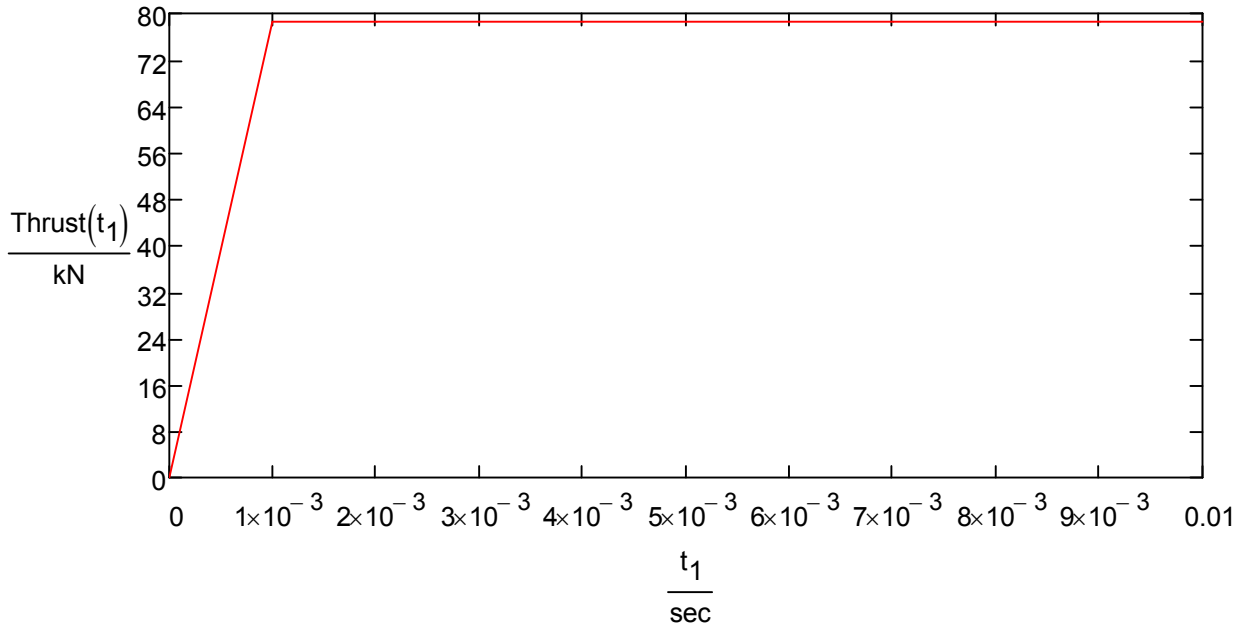

Figure B.4 - Break thrust force time-history initial trust

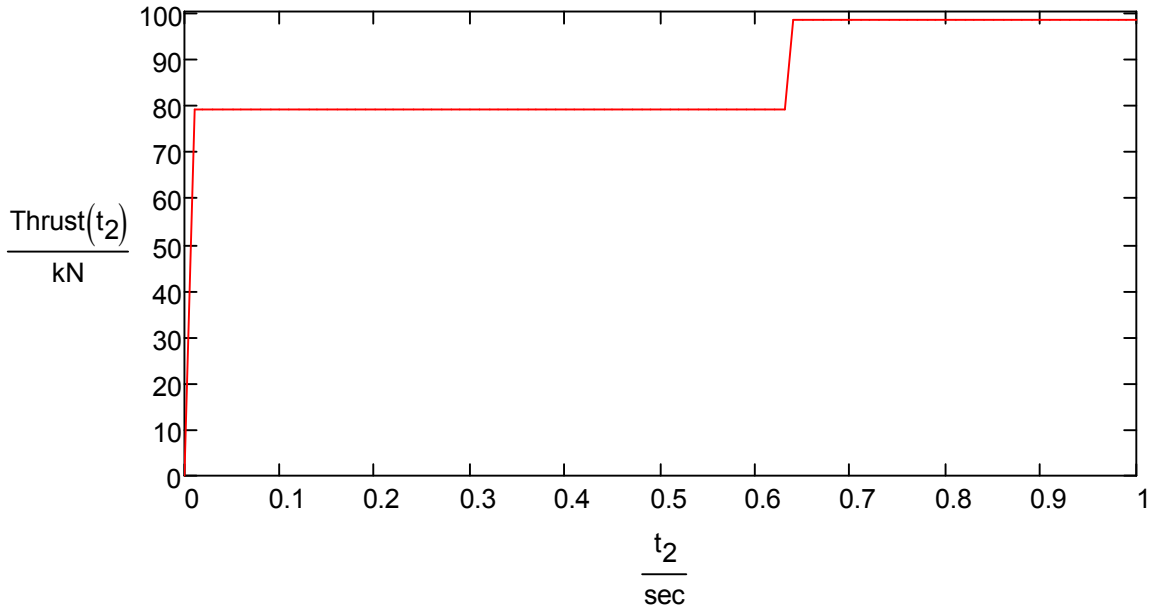

Figure B.5 - Break thrust force time-history initial and steady-state force

Appendix C

U-Bar design calculation
(extracted from PTC Mathcad file)

Nomenclature (PTC, 2007)

A_t	Total area of tension members	(m^2)	
A_{t_act}	Actual total area of U-bar	(m^2)	
A_{U_Bar}	Area of U-bar	(m^2)	
DLF	Dynamic load factor	(dimensionless)	
d_t	Plastic deformation of tension members	(m)	
d_{U_bar}	Minimum diameter of U-bar	(m)	
$d_{U\_bar\_Act}$	Standard U-bar rod diameter	(m)	
F_e	Equivalent thrust resultant	(kN)	
F_T	Actual transmitted load	(kN)	
Gap	Distance between PWR and pipe	(m)	
$Length_{U\_Bar}$	Distance between center of pipe and the backup structure	(m)	
L_{hinge}	Length of the dynamic hinge	(m)	(Roemer and East, 1980)
L_1	Distance from hinge to pipe whip restraint	(m)	
L_3	From hinge point to static plastic hinge point	(m)	
L_4	Distance that the PWR should be placed	(m)	
L_S	Static plastic hinge length	(m)	
M_p	Plastic moment	(kN.m)	(Roemer and East, 1980)
M_s	Steady-state moment	(kN.m)	
n	Number of round bars	(dimensionless)	
r_o	Pipe outside radius	(m)	(ASME, 2004f)
S_{y1}	Static metal yield stress – Round bar	(MPa)	(ASME, 2004a)
S_{y2}	Static metal yield stress – Pipe	(MPa)	(ASME, 2004a)
S_{YD}	Dynamic metal yield design stress	(MPa)	(ANS, 1998)

t	Pipe wall thickness	(m)	(ASME, 2004f)
T_{INT}	Initial thrust force	(kN)	(ANS, 1998)
T_{max}	Maximum thrust force	(kN)	
T_{SS}	Steady-state thrust force at time t_{ss}	(kN)	(ANS, 1998)
T_{thrust}	Maximum thrust	(kN)	(ANS, 1998)
x	Distance from elbow to pipe whip restraint	(m)	
Z_p	Plastic section modulus	(m^3)	
ε_u	Strain	(dimensionless)	
σ_{yield_max}	Maximum yield stress	(MPa)	

List of equations

Equivalent thrust resultant at PWR:

$$F_e(T_{thrust}, L, L_1) := 1.1 \cdot T_{thrust} \cdot \left(\frac{L}{L_1}\right) \quad \text{(C1)}$$

Maximum thrust force:

$$T_{max}(T_{INT}, T_{SS}) := \max(T_{INT}, T_{SS}) \quad \text{(C2)}$$

Plastic deformation of tension members:

$$d_t(\varepsilon_u, Lenght_{U\_Bar}) := 0.5 \cdot \varepsilon_u \cdot Lenght_{U\_Bar} \quad \text{(C3)}$$

Total area of tension members:

$$A_t(F_e, Gap, d_t, S_{yd}) := \frac{F_e \cdot (Gap + d_t)}{d_t \cdot S_{yd}} \quad \text{(C4)}$$

Area of U-bar:

$$A_{U\_Bar}(A_t, n) := \frac{A_t}{2n} \quad \text{(C5)}$$

Minimum diameter of u-bar:

$$d_{U\_Bar}(A_{U\_Bar}) := \sqrt{\frac{A_{U\_Bar} \cdot 4}{\pi}} \quad \text{(C6)}$$

Actual total area of U-bar:

$$A_{t\_act}(d_{U\_Bar\_Act}, n) := \frac{\pi \cdot d_{U\_Bar\_Act}^{2} \cdot 2 \cdot n}{4} \quad \text{(C7)}$$

Actual transmitted load to support structure:

$$F_T(\sigma_{yield\_max}, A_{t\_act}) := 1.1 \sigma_{yield\_max} \cdot A_{t\_act} \quad \text{(C8)}$$

Plastic section modulus:

$$Z_p(r_o, r_i) := \frac{4}{3}\left(r_o^{3} - r_i^{3}\right) \quad \text{(C9)}$$

Steady-state moment:

$$M_s(S_y, Z_p) := S_y \cdot Z_p \quad \text{(C10)}$$

Steady-state length:

$$L_s(M_s, F_e) := \frac{M_s}{F_e} \quad \text{(C11)}$$

Dynamic thrust:

$$T_{thrust}(T_{max}, DLF) := T_{max} \cdot DLF \quad \text{(C12)}$$

Inputs:

$DLF := 2$	(ANS, 1998)
$L_{hinge} := 2.2\,m$	(Appendix B)
$T_{INT} := 78.68\ kN$	(Appendix B)
$T_{SS} := 98.34\ kN$	(Appendix B)
$S_{y1} := 206.84\ MPa$	(ASME, 2004a)
$S_{y2} := 173.06\ MPa$	(ASME, 2004a)
$\sigma_{yield\_max} := 255.11\ MPa$	(ASME, 2004a)
$\varepsilon_u := 0.40$	(ASME, 2004a)
$M_p := 78.581\ kN \cdot m$	(Appendix B)
$r_i := 65.88\ mm$	(Appendix B)
$r_o := 84.14\ mm$	(Appendix B)
$Length_{U\_Bar} := 300\ mm$	Distance between center of pipe and attachment to backup structure (tension member length)
$L_1 := 1.95\,m$	Assume L_1 for first iteration
$Gap := 50\,mm$	Gap distance between pipe and restraint
$n := 4$	Number of U-bars (2 tension members each)

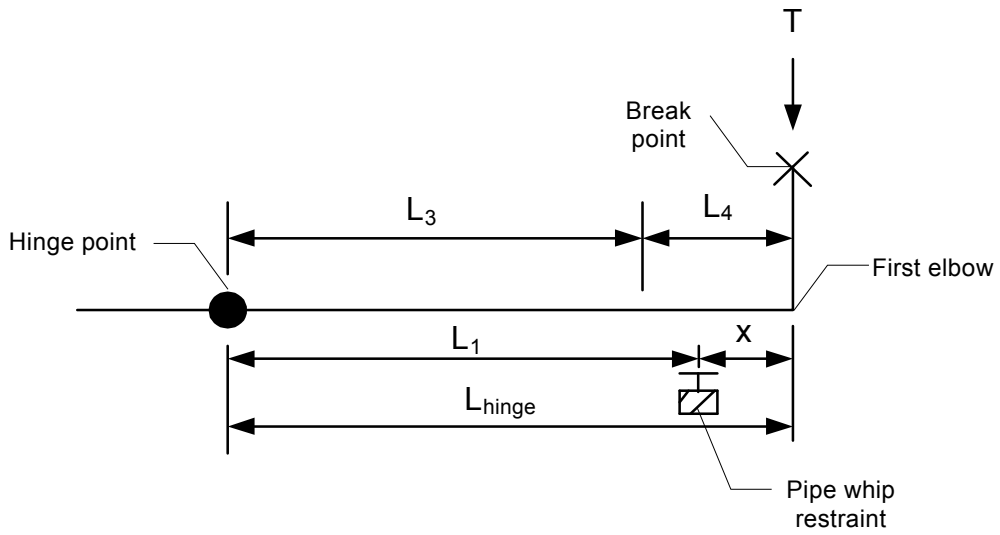

Figure C.1 - Simplified piping and whip restraint geometry

C.1: Calculation of U-bar diameter and transmitted load:

$S_{yd} := 1.1 \cdot S_{y1}$ Add 10% due to high strain rate deformation (ANS, 1998)

Applying equation C2:

$T_{max}(T_{INT}, T_{SS}) = 98.34 \cdot kN$ (ANS, 1998)

Applying equation C3:

$d_t(\varepsilon_u, \text{Length}_{U\_Bar}) = 60 \cdot mm$ (Hearn, 2000)

Applying equation C1:

$F_e(T_{thrust}(T_{max}(T_{INT}, T_{SS}), DLF), L_{hinge}, L_1) = 244.08 \cdot kN$ (Chapter 3)

Determine the steady-state hinge length:

Applying equation C2:

$M_s(S_{y2}, Z_p(r_o, r_i)) = 71.47 \cdot kN \cdot m$

Applying equation C11:

$$L_{s.} := \frac{M_s(S_{y2}, Z_p(r_o, r_i))}{F_e(T_{thrust}(T_{max}(T_{INT}, T_{SS}), DLF), L_{hinge}, L_1)} = 0.29\,m$$

Ensure that the x is smaller than L_s:

$x := L_{hinge} - L_1 = 0.25\,m$

The steady-state hinge is longer than the allowable distance x, therefore no secondary hinge is anticipated after the break.

Applying equation C4:

$$A_t\left(F_e\left(T_{thrust}\left(T_{max}\left(T_{INT}, T_{SS}\right), DLF\right), L_{hinge}, L_1\right), Gap, d_t\left(\varepsilon_u, Length_{U\_Bar}\right), S_{yd}\right) = 1966.78\ \cdot mm^2$$

Define formula simpler:

$$A_{t1} := A_t\left(F_e\left(T_{thrust}\left(T_{max}\left(T_{INT}, T_{SS}\right), DLF\right), L_{hinge}, L_1\right), Gap, d_t\left(\varepsilon_u, Length_{U\_Bar}\right), S_{yd}\right)$$

Applying equation C5:

Use factor 2 because of two sides for each U-bar

$$A_{U\_Bar}\left(A_{t1}, n\right) = 245.85\ \cdot mm^2$$

Applying equation C6:

Calculated minimum diameter of U-Bar

$$d_{U\_Bar}\left(A_{U\_Bar}\left(A_{t1}, n\right)\right) = 17.69\ \cdot mm$$

Select next higher standard size rod:

$$d_{U\_Bar\_Act} := 20\,mm$$

Actual total area

Applying equation C7:

$$A_{t\_act}\left(d_{U\_Bar\_Act}, n\right) = 2513.27\ \cdot mm^2$$

Actual transmitted load to backup support structure

Applying equation C7:

$$F_T\left(\sigma_{yield\_max}, A_{t\_act}\left(d_{U\_Bar\_Act}, n\right)\right) = 705.28\ \cdot kN$$

Appendix D

Crush pipe design calculation
(extracted from PTC Mathcad file)

Nomenclature (PTC, 2007)

C_1	Collapse deformation (Simplicity symbol for 1st iteration)	(m)	(Spada and Goldstein, 1980)
C_2	Collapse deformation (Simplicity symbol for 2nd iteration)	(m)	(Spada and Goldstein, 1980)
C_3	Collapse deformation (Simplicity symbol for 3rd iteration)	(m)	(Spada and Goldstein, 1980)
D_b	Bumper diameter	(m)	(Spada and Goldstein, 1980)
D_{b1}	Bumper diameter 2nd iteration	(m)	(Spada and Goldstein, 1980)
D_{b2}	Bumper diameter 3rd iteration	(m)	(Spada and Goldstein, 1980)
D_e	Pipe inside diameter	(m^2)	(ANS, 1998)
D_p	Crush pipe diameter	(m)	(Spada and Goldstein, 1980)
E	Young's modulus	(GPa)	(Hearn, 2000)
F_c	Deformation force	(kN)	(Spada and Goldstein, 1980)
$F_{ci} = F_p$	Empirical scaling force	(kN)	(Spada and Goldstein, 1980)
F_{cr}	Crush pipe force (Formula)	(kN)	(Spada and Goldstein, 1980)
F_{cr1}	Crush pipe force (value only)	(kN)	(Spada and Goldstein, 1980)
g_m	Motion parallel to bumper	(m)	(Spada and Goldstein, 1980)
K_{1r}	Elastic ring stiffness	(kN/m)	(Spada and Goldstein, 1980)
K_{2r}	Plastic ring stiffness	(kN/m)	(Spada and Goldstein, 1980)
L_c	Length of crush pipe $D_b \geq D_p$	(m)	(Spada and Goldstein, 1980)
l_e	Final length of crush pipe	(m)	(Spada and Goldstein, 1980)
L_{cp}	Length of crush pipe $D_b \leq D_p$	(m)	(Spada and Goldstein, 1980)
L_{sp}	Length of support structure	(m)	(Spada and Goldstein, 1980)
r_b	Mean radius of crush pipe	(m)	(Spada and Goldstein, 1980)

r_{b1}	Mean radius of crush pipe (2nd iteration)	(m)	(Spada and Goldstein, 1980)
r_{b2}	Mean radius of crush pipe (3rd iteration)	(m)	(Spada and Goldstein, 1980)
r_p	Mean radius of process pipe	(m)	(Spada and Goldstein, 1980)
t_e	Wall thickness of crush pipe (empirical)	(in)	(Spada and Goldstein, 1980)
t_b	Wall thickness of crush pipe	(m)	(Spada and Goldstein, 1980)
t_{b1}	Wall thickness of crush pipe (2nd iteration)	(m)	(Spada and Goldstein, 1980)
t_{b2}	Wall thickness of crush pipe (3rd iteration)	(m)	(Spada and Goldstein, 1980)
t_{cp}	Minimum wall thickness of crush pipe	(m)	(Spada and Goldstein, 1980)
t_p	Wall thickness of process pipe	(m)	(Spada and Goldstein, 1980)
Δ_c	Collapse deformation	(m)	(Spada and Goldstein, 1980)
σy	Allowable yield stress	(GPa)	(Hearn, 2000)

List of equations

Length of the crush pipe for $D_b \le D_p$

$$L_{cp}(D_b, D_p, g_m) := 2 \cdot D_b + D_p + 2 \cdot g_m \quad \text{(D1)}$$

Length of the crush pipe for $D_b \ge D_p$

$$L_c(D_b, g_m) := 3 \cdot D_b + 2.g_m \quad \text{(D2)}$$

Length of the support structure

$$L_{sp}(D_b, g_m) := 2.5 \cdot D_b + 2 \cdot g_m \quad \text{(D3)}$$

Minimum thickness of the crush pipe

$$t_{cp}(t_p, r_b, r_p) := 0.75 \cdot t_p \cdot \left(\frac{r_b}{r_p}\right)^{0.131} \quad \text{(D4)}$$

Deformation Force

$$F_c(F_{cr1}, F_{ci}) := F_{cr1} + F_{ci} \quad \text{(D5)}$$

Crush pipe force

$$F_{CR}(K_{1r}, \Delta_c) := K1r.\Delta_c \quad \text{(D6)}$$

Empirical scaling law for force

$$F_p(t_e, D_e) := 35000 \cdot \left(\frac{t_e}{0.349}\right)^2 \cdot \left(\frac{4.5}{D_e}\right)^{0.27} \quad \text{(D7)}$$

Elastic ring stiffness

$$K_{1r}(E, I_e, t_b, D_b) := 4.48 \cdot E \cdot I_e \cdot \frac{\left(\frac{t_b}{D_b}\right)^3}{\left(1 - \frac{t_b}{D_b}\right)^3} \quad \text{(D8)}$$

Plastic ring stiffness

$$K_{2r}(\sigma_y, l_e, t_b, D_b) := 4.86 \cdot \sigma_y \cdot l_e \cdot \frac{\left(\frac{t_b}{D_b}\right)^2}{\left(1 - \frac{t_b}{D_b}\right)} \tag{D9}$$

Collapse deformation of crush pipe

$$\Delta_c(\sigma_y, l_e, t_b, D_b, K_{1r}, K_{2r}) := 40 \cdot \sigma_y \cdot l_e \cdot t_b \cdot \frac{\left(\frac{t_b}{D_b}\right)^2 \cdot \left(1 - \frac{t_b}{D_b}\right)}{K_{1r} - K_{2r}} \tag{D10}$$

Process pipe inside radius

$$r_p(D_p) := \frac{D_p}{2} \tag{D11}$$

Crush pipe inside radius

First consideration pipe

$$r_b(D_b) := \frac{D_b}{2} \tag{D12}$$

Second consideration pipe

$$r_{b1}(D_{b1}) := \frac{D_{b1}}{2} \tag{D13}$$

Third consideration pipe

$$r_{b2}(D_{b2}) := \frac{D_{b2}}{2} \tag{D14}$$

Inputs:

$D_b := 131.75\ mm$		(ASME, 2004f)
$D_{b1} := 114.3\ mm$		(ASME, 2004f)
$D_{b2} := 219.1\ mm$		(ASME, 2004f)
$D_p := 168.3\ mm$		(ASME, 2004f)
$t_b := 14.27\ mm$		(ASME, 2004f)
$t_{b1} := 11.13\ mm$		(ASME, 2004f)
$t_{b2} := 18.26\ mm$		(ASME, 2004f)
$t_p := 18.26\ mm$		(ASME, 2004f)
$E := 175.82\ GPa$		(ASME, 2004a)
$\sigma_y := 0.173\ GPa$	SA − 333 Gr 6	(ASME, 2004a)

D.1 Crush Pipe dimensions:

Pipe is 150NB, schedule 160 (ASME, 2004f)

The pipe variables are visually indicated in **Figure D.1**

From equation D11:

$r_p(D_p) = 84.15 \cdot mm$

Crush Pipe is 150NB, schedule 120 (ASME, 2004f)

The pipe variables are visually indicated in **Figure D.2**

From equation D12:

$r_b(D_b) = 65.88 \cdot mm$

Crush Pipe is 100NB, schedule 120 (ASME, 2004f)

The pipe variables are visually indicated in **Figure D.2**

From equation D13:

$r_{b1}(D_{b1}) = 57.15 \cdot mm$

Crush Pipe is 200NB, schedule 120 (ASME, 2004f)

The pipe variables are visually indicated in **Figure D.2**

From equation D14:

$r_{b2}(D_{b2}) = 109.55 \cdot mm$

$g_m := 0m$

From equation D1:

$L_{cp}(D_b, D_p, g_m) = 431.8 \cdot mm$ (Spada and Goldstein, 1980)

From equation D2:

$L_c(D_b, g_m) = 395.25 \cdot mm$ (Spada and Goldstein, 1980)

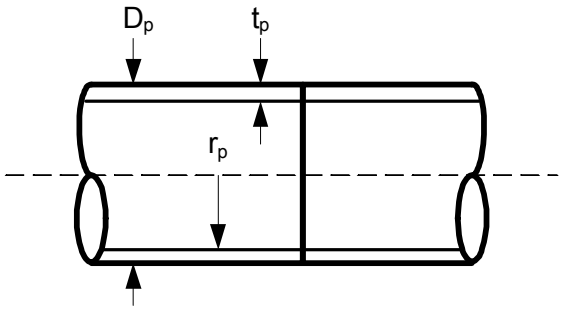

Figure D.1 - Process pipe dimensions

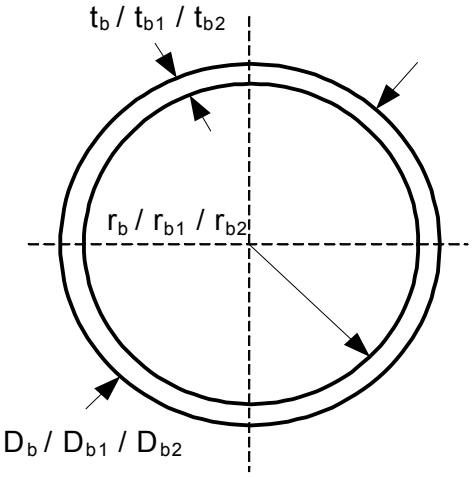

Figure D.2 - Crush pipe dimensions

From equation D3:

$L_{sp}(D_b, g_m) = 329.38 \cdot mm$ (Spada and Goldstein, 1980)

From equation D4:

$t_{cp}(t_p, r_b(D_b), r_p(D_p)) = 13.26 \cdot mm$ (Spada and Goldstein, 1980)

D.2 Empirical pipe force 150NB Schedule 120

Empirical scaling law for crush force of process pipe:

$t_e := 0.719 \ Inch \quad (t_e = t_p)$ (Enis, Bernal and Burdette, 1980)

$D_e := 6.625 \ Inch \quad (D_e = D_p)$ (Enis, Bernal and Burdette, 1980)

From equation D7:

$F_p(t_e, D_e) = 133820.35 \ lbf$ (Enis, Bernal and Burdette, 1980)

$133820.35 \ lbf = 595.26 \cdot kN$

$F_{ci} := 595.26 \, kN$

Elastic ring stiffness:

From equation D8:

$I_e := L_{cp}(D_b, D_p, g_m)$

$K_{1r}(E, I_e, t_b, D_b) = 609549.58 \cdot \frac{kN}{m}$ (Enis, Bernal and Burdette, 1980)

Plastic ring stiffness:

From equation D9:

$K_{2r}(\sigma_y, I_e, t_b, D_b) = 4776.37 \cdot \frac{kN}{m}$ (Enis, Bernal and Burdette, 1980)

Collapse deformation of crush pipe:

From equation D10: (Enis, Bernal and Burdette, 1980)

$$\Delta_c\left(\sigma_y, I_e, t_b, D_b, K_{1r}\left(E, I_e, t_b, D_b\right), K_{2r}\left(\sigma_y, I_e, t_b, D_b\right)\right) = 0.74 \cdot mm$$

For simplicity:

$$C_1 := \Delta_c\left(\sigma_y, I_e, t_b, D_b, K_{1r}\left(E, I_e, t_b, D_b\right), K_{2r}\left(\sigma_y, I_e, t_b, D_b\right)\right)$$

Therefore for the crush pipe force:

From equation D6:

$$F_{cr}\left(K_{1r}\left(E, I_e, t_b, D_b\right), C_1\right) = 449.56 \cdot kN$$

Define value for ease of calculation:

$$F_{cr1} := 449.56 \quad kN$$

Pipe crush force:

From equation D5:

$$F_c\left(F_{cr1}, F_{ci}\right) = 1044.82 \cdot kN$$

D.3 Empirical pipe force 100NB Schedule 120

Elastic ring stiffness:

$$K_{1r}\left(E, I_e, t_{b1}, D_{b1}\right) = 427025.81 \cdot \frac{kN}{m}$$ (Enis, Bernal and Burdette, 1980)

Plastic ring stiffness:

From equation D9:

$$K_{2r}\left(\sigma_y, I_e, t_{b1}, D_{b1}\right) = 3813.78 \cdot \frac{kN}{m}$$ (Enis, Bernal and Burdette, 1980)

Collapse deformation of crush pipe:

From equation D10: (Enis, Bernal and Burdette, 1980)

$$\Delta_c\left(\sigma_y, I_e, t_{b1}, D_{b1}, K_{1r}\left(E, I_e, t_{b1}, D_{b1}\right), K_{2r}\left(\sigma_y, I_e, t_{b1}, D_{b1}\right)\right) = 0.67 \cdot mm$$

For simplicity:

$$C_2 := \Delta_c\left(\sigma_y, I_e, t_{b1}, D_{b1}, K_{1r}\left(E, I_e, t_{b1}, D_{b1}\right), K_{2r}\left(\sigma_y, I_e, t_{b1}, D_{b1}\right)\right)$$

Therefore for the crush pipe force:

From equation D6:

$$F_{cr}\left(K_{1r}\left(E, I_e, t_{b1}, D_{b1}\right), C_2\right) = 287.2 \cdot kN$$

Pipe crush force:

From equation D5:

$$F_c\left(F_{cr}\left(K_{1r}\left(E, I_e, t_{b1}, D_{b1}\right), C_2\right), F_{ci}\right) = 882.46 \cdot kN$$

D.4 Empirical pipe force 200NB Schedule 120

$l_{e.} := L_c(D_b, g_m)$

Elastic ring stiffness:

$K_{1r}(E, l_{e.}, t_{b2}, D_{b2}) = 233975.21 \cdot \frac{kN}{m}$ (Enis, Bernal and Burdette, 1980)

Plastic ring stiffness:

From equation D9:

$K_{2r}(\sigma_y, l_{e.}, t_{b2}, D_{b2}) = 2518.04 \cdot \frac{kN}{m}$ (Enis, Bernal and Burdette, 1980)

Collapse deformation of crush pipe:

From equation D10: (Enis, Bernal and Burdette, 1980)

$\Delta_c(\sigma_y, l_{e.}, t_{b2}, D_{b2}, K_{1r}(E, l_{e.}, t_{b2}, D_{b2}), K_{2r}(\sigma_y, l_{e.}, t_{b2}, D_{b2})) = 1.37 \cdot mm$

For simplicity:

$C_3 := \Delta_c(\sigma_y, l_{e.}, t_{b2}, D_{b2}, K_{1r}(E, l_{e.}, t_{b2}, D_{b2}), K_{2r}(\sigma_y, l_{e.}, t_{b2}, D_{b2}))$

Therefore for the crush pipe force:

From equation D6:

$F_{cr}(K_{1r}(E, l_{e.}, t_{b2}, D_{b2}), C_3) = 321.44 \cdot kN$

Pipe crush force:

From equation D5:

$F_c(F_{cr}(K_{1r}(E, l_{e.}, t_{b2}, D_{b2}), C_3), F_{ci}) = 916.7 \cdot kN$

Appendix E

Crush pipe design calculation-energy method (extracted from PTC Mathcad file)

Nomenclature (PTC, 2007)

a	Quadratic symbol	(dimensionless)	(Gieck and Gieck, 1996)
b	Quadratic symbol	(dimensionless)	(Gieck and Gieck, 1996)
D_b	Bumper diameter	(m)	(Spada and Goldstein, 1980)
DLF	Dynamic load factor	(dimensionless)	
D_p	Crush pipe diameter	(m)	(Spada and Goldstein, 1980)
c_1	Quadratic symbol	(dimensionless)	(Gieck and Gieck, 1996)
E	Young's modulus	(GPa)	(Hearn, 2000)
F_1	Deformation force	(kN)	(Spada and Goldstein, 1980)
F_t	Total force	(kN)	
F_y	Force at yield	(kN)	(Hearn, 2000)
F_{yield}	Force at yield (Graph)	(kN)	(Hearn, 2000)
g_m	Motion parallel to bumper	(m)	(Spada and Goldstein, 1980)
k_1	Elastic ring stiffness (Value only)	(kN/m)	(Spada and Goldstein, 1980)
k_2	Plastic ring stiffness (Value only)	(kN/m)	(Spada and Goldstein, 1980)
K_1	Elastic ring stiffness (Formula)	(kN/m)	(Spada and Goldstein, 1980)
K_2	Plastic ring stiffness (Formula)	(kN/m)	(Spada and Goldstein, 1980)
l_1	Distance from dynamic hinge to PWR	(m)	
l_2	Dynamic hinge length	(m)	
L_c	Length of crush pipe $D_b \geq D_p$	(m)	(Spada and Goldstein, 1980)
l_e	Effective length of crush pipe	(m)	(Spada and Goldstein, 1980)

L_{cp}	Length of crush pipe $D_b \leq D_p$	(m)	(Spada and Goldstein, 1980)
L_{sp}	Length of support structure	(m)	(Spada and Goldstein, 1980)
r_b	Mean radius of crush pipe	(m)	(Spada and Goldstein, 1980)
r_p	Mean radius of process pipe	(m)	(Spada and Goldstein, 1980)
t_b	Wall thickness of crush pipe	(m)	(Spada and Goldstein, 1980)
t_p	Wall thickness of process pipe	(m)	(Spada and Goldstein, 1980)
T_{SS}	Steady-state thrust force at time t_{ss}	(kN)	(ANS, 1998)
T_{DYN}	Dynamic thrust force	(kN)	(ANS, 1998)
U	Potential energy	(J)	(Boresi and Schimdt, 2003)
U_m	Strain energy	(J)	(Boresi and Schimdt, 2003)
U_y	Potential energy at yield	(J)	
δ_C	Maximum deformation of crush pipe at yield (Formula)	(m)	(Spada and Goldstein, 1980)
δ_c	Maximum deformation of crush pipe at yield (Value)	(m)	(Spada and Goldstein, 1980)
δ_G	Effective gap distance of travel	(m)	
δ_{Ma}	Maximum collapse deformation of crush pipe (positive)	(m)	
δ_{Mb}	Maximum collapse deformation of crush pipe (negative)	(m)	
σy	Allowable yield stress	(GPa)	(Hearn, 2000)

List of equations

Length of the crush pipe for $D_b \le D_p$

$$L_{cp}(D_b, D_p, g_m) := 2 \cdot D_b + D_p + 2 \cdot g_m \tag{E1}$$

Length of the crush pipe for $D_b \ge D_p$

$$L_c(D_b, g_m) := 3 \cdot D_b + 2 \cdot g_m \tag{E2}$$

Length of the support structure

$$L_{sp}(D_b, g_m) := 2.5 \cdot D_b + 2 \cdot g_m \tag{E3}$$

Strain energy

$$U_m(T_{DYN}, l_2, l_1) := \frac{1}{2} \cdot 1.1 \cdot l_2 \cdot T_{DYN} \cdot \frac{l_2}{l_1} \tag{E4}$$

Potential energy

$$U(F_t, l_2, l_1) := \frac{1}{2} \cdot l_1 \cdot F_t \cdot \frac{l_1}{l_2} \tag{E5}$$

Potential energy at yield

$$U_y(F_y, l_2, l_1) := \frac{1}{2} \cdot l_1 \cdot F_y \cdot \frac{l_1}{l_2} \tag{E6}$$

Elastic ring stiffness of crush pipe

$$K_{.1}(E, l_{.e}, t_{.b}, D_{.b}) := 4.48 \cdot E \cdot l_{.e} \cdot \left[\frac{\left(\frac{t_{.b}}{D_{.b}} \right)^3}{\left(1 - \frac{t_{.b}}{D_{.b}} \right)^3} \right] \tag{E7}$$

Plastic ring stiffness of crush pipe

$$K_2(\sigma_y, l_e, t_b, D_b) := 4.86 \cdot \sigma_y \cdot l_e \cdot \left[\frac{\left(\frac{t_b}{D_b} \right)^2}{\left(1 - \frac{t_b}{D_b} \right)} \right] \tag{E8}$$

Maximum deformation of crush pipe at yield

$$\delta_C(\sigma_y, l_e, t_b, D_b, K_1, K_2) := \frac{40 \cdot \sigma_y \cdot l_e \cdot t_b \cdot \left(\frac{t_b}{D_b} \right)^2 \cdot \left(1 - \frac{t_b}{D_b} \right)}{K_1 - K_2} \tag{E9}$$

Process pipe inside radius

$$r_p(D_p, t_p) := \frac{D_p - 2 \cdot t_p}{2} \tag{E10}$$

Crush pipe inside radius

$$r_b(D_b, t_b) := \frac{(D_b - 2 \cdot t_b)}{2} \tag{E11}$$

Maximum deformation of the crush pipe

$$\delta_{Ma}(b, a, c_1) := \frac{-b + \sqrt{b^2 - 4 \cdot a \cdot c_1}}{2 \cdot a} \tag{E12}$$

$$\delta_{Mb}(b, a, c_1) := \frac{-b - \sqrt{b^2 - 4 \cdot a \cdot c_1}}{2 \cdot a} \tag{E13}$$

where:

$$a(k_2) := \frac{1}{2} \cdot k_2 \tag{E14}$$

$$b(T_{DYN}, k_1, \delta_C) := -1.1 \cdot T_{DYN} + (k_1 \cdot \delta_C) \tag{E15}$$

$$c_1(T_{DYN}, k_1, \delta_C, k_2, \delta_G) := -1.1 \cdot T_{DYN} \cdot \delta_G + \frac{1}{2} \cdot (k_2 - k_1) \cdot \delta_C^{\,2} \tag{E16}$$

Inputs:

$D_b := 10.75\ in = 273.05\ mm$ (ASME, 2004f, 250NB)

$D_p := 168.3\ mm$ (ASME, 2004f; 150NB Schedule 160)

$DLF := 2$ (ANS, 1998)

$E := 29500000\ psi = 203395.34\ MPa$ (ASME, 2004a)

$l_1 := 1.95\ m$ Distance from dynamic hinge to PWR

$l_2 := 2.2\ m$ Dynamic hinge length - Appendix B

$T_{SS} := 98.34\ kN$ Appendix B

$t_b := 0.365\ in = 9.27\ mm$ (ASME, 2004f; 250NB Schedule 60)

$t_p := 18.26\ mm$ (ASME, 2004f; 150NB Schedule 160)

$\sigma_y := 35000\ psi = 241.32\ MPa$ (ASME, 2004a; SA - 333 Grade 6)

$\delta_G := 50\ mm$ (Appendix B)

$g_m := 0\ m$

E.1 Process pipe dimensions:

Pipe is 150NB, schedule 160 (ASME, 2004f)

The pipe variables are visually indicated in **Figure E.1**.

From equation E10:

$r_p(D_p, t_p) = 65.89 \cdot mm$

E.2 Crush pipe dimensions:

Crush pipe is 250NB, schedule 80 (ASME, 2004f)

The pipe variables are visually indicated in **Figure E.2**.

From equation E11:

$r_b(D_b, t_b) = 127.25 \cdot mm$

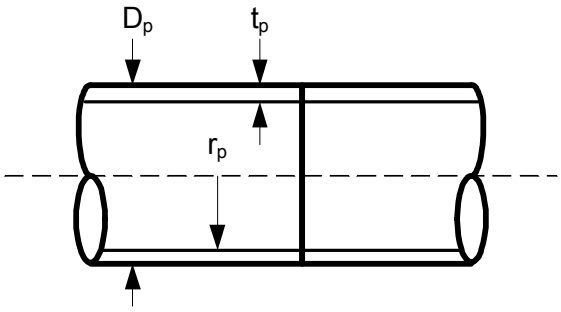

Figure E.1 - Process pipe dimensions

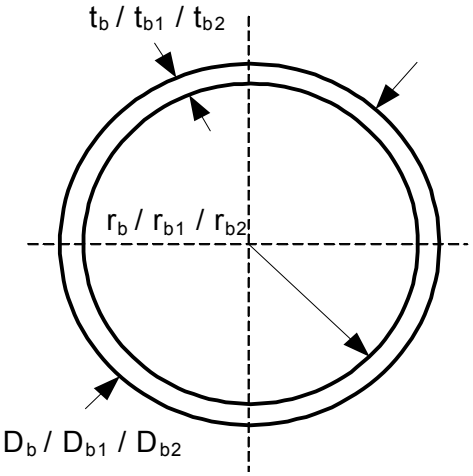

Figure E.2 - Crush pipe dimensions

E.3 Strain energy for 150NB Schedule 160 process pipe

Dynamic thrust force

$T_{DYN} := T_{SS} \cdot DLF$

$T_{DYN} = 196.68 \cdot kN$

From equation E4:

$U_m(T_{DYN}, l_2, l_1) = 268.49 \cdot kJ$

E.4 Potential energy for 250NB crush pipe

Length of the support structure:

From equation E3:

$L_{sp}(D_b, g_m) = 682.63 \cdot mm$ (Spada and Goldstein, 1980)

Length of the crush pipe:

From equation E1:

$L_{cp}(D_b, D_p, g_m) = 714.4 \cdot mm$ (Spada and Goldstein, 1980)

Schedule 80:

$l_e := D_p$ (Enis, Bernal and Burdette, 1980)

$l_e = 168.3 \cdot mm$

Elastic ring stiffness:

From equation E7:

$K_1(E, l_e, t_b, D_b) = 38019.77 \cdot \frac{lbf}{in}$ (Enis, Bernal and Burdette, 1980)

$K_1(E, l_e, t_b, D_b) = 6658.28 \cdot \frac{kN}{m}$

Plastic ring stiffness:

From equation E8:

$K_2(\sigma_y, l_e, t_b, D_b) = 1345.01 \cdot \frac{lbf}{in}$ (Enis, Bernal and Burdette, 1980)

$K_2(\sigma_y, l_e, t_b, D_b) = 235.55 \cdot \frac{kN}{m}$

Deformation at maximum yield:

From equation E9:

$\delta_C(\sigma_y, l_e, t_b, D_b, K_1(E, l_e, t_b, D_b), K_2(\sigma_y, l_e, t_b, D_b)) = 2.61 \cdot mm$

For simplicity define functions in shorter notation:

$k_1 := K_1(E, l_e, t_b, D_b)$

$k_2 := K_2(\sigma_y, l_e, t_b, D_b)$

$\delta_c := \delta C(\sigma_y, l_e, t_b, D_b, K_1(E, l_e, t_b, D_b), K_2(\sigma_y, l_e, t_b, D_b))$

Force at yield:

$F_y := k_1 \cdot \delta_c$ (Hearn, 2000)

$F_y = 17.39 \cdot kN$

Energy at yield:

From equation E6:

$U_y(F_y, l_2, l_1) = 15.03 \cdot kJ$

Indication of the yield force to deflection at yield:

$\delta_{yield} := 0 \cdot mm, .001\,mm .. 0.01 \cdot mm$

$F_{yield}(\delta_c) := \Phi(1 \cdot 10^{-3} mm - \delta_c) \cdot \left(\frac{F_y}{1 \cdot 10^{-3} \cdot mm} \cdot \delta_c \right) + \Phi(\delta_c - 1 \cdot 10^{-3} mm) \cdot F_y$

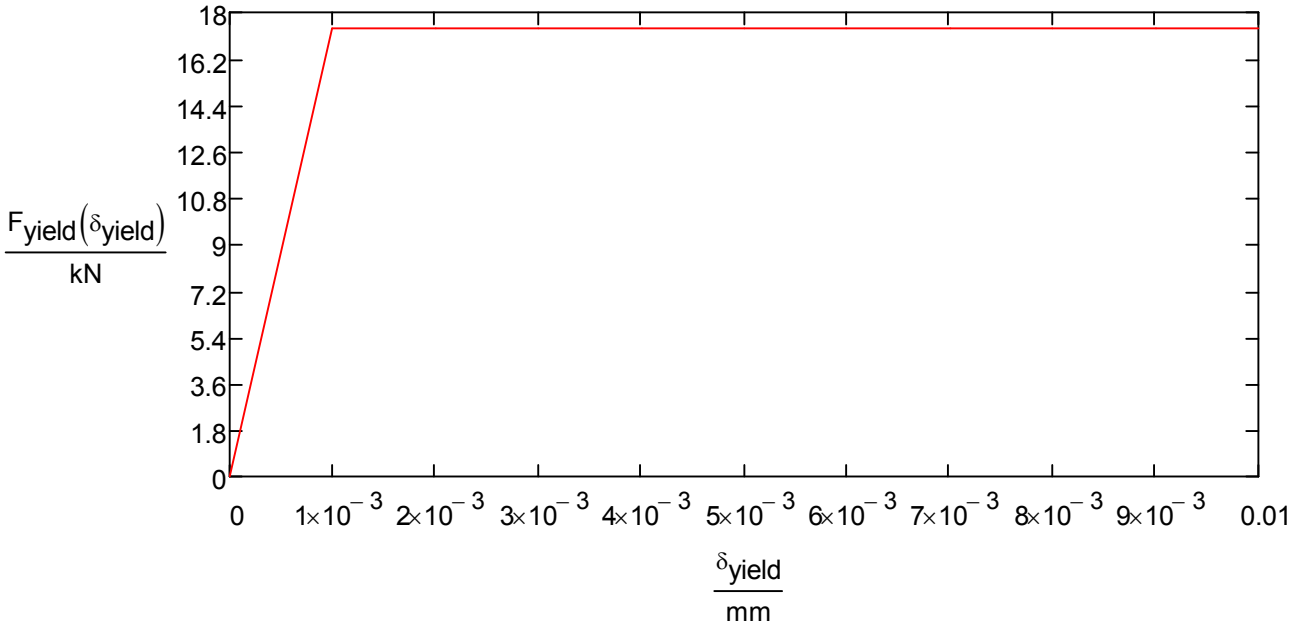

Figure E.3 - Force at yield

Crush force of pipe:

From equation E14:

$$a(k_2) = 672.5 \cdot \frac{lbf}{in}$$

$$a(k_2) = 117.77 \cdot \frac{kN}{m}$$

From equation E15:

$$b(T_{DYN}, k_1, \delta_c) = -44727.83 \cdot lbf$$

$$b(T_{DYN}, k_1, \delta_c) = -198.96 \cdot kN$$

From equation E16:

$$c_1(T_{DYN}, k_1, \delta_c, k_2, \delta_G) = -95935.91 \cdot lbf \cdot in$$

$$c_1(T_{DYN}, k_1, \delta_c, k_2, \delta_G) = -10.84 \cdot kN \cdot m$$

From equation E12:

$$\delta_{Ma}(b(T_{DYN}, k_1, \delta_c), a(k_2), c_1(T_{DYN}, k_1, \delta_c, k_2, \delta_G)) = 1742.16 \cdot mm$$

From equation E13:

$$\delta_{Mb}(b(T_{DYN}, k_1, \delta_c), a(k_2), c_1(T_{DYN}, k_1, \delta_c, k_2, \delta_G)) = -52.83 \cdot mm$$

$$F_1 := k_1 \cdot |\delta_{Mb}(b(T_{DYN}, k_1, \delta_c), a(k_2), c_1(T_{DYN}, k_1, \delta_c, k_2, \delta_G))|$$

$$F_1 = 351.74 \cdot kN$$

$$F_t := F_1 - F_y$$

From equation E5:

$$U(F_t, l_2, l_1) = 288.95 \cdot kJ$$

Appendix F

Crush pipe validation keyword cards
(extracted from LS-PrePost® file)

Material models:

*MAT_PIECEWISE_LINEAR_PLASTICITY: Elastic perfectly plastic option

*MAT_RIGID_TITLE: Backing plate

*LOAD_NODE_POINT: Follower force option

*CONSTRAINED_NODAL_RIGID_BODY: Rigid body used to transfer the load from the application node to the pipe

Contact:

*CONTACT_AUTOMATIC_SURFACE_TO_SURFACE_ID

Keywords used:

*KEYWORD

*TITLE

*CONTROL_TERMINATION

*DATABASE_BINARY_D3PLOT

*BOUNDARY_SPC_NODE

*LOAD_NODE_POINT

*CONTACT_AUTOMATIC_SURFACE_TO_SURFACE_ID

*MAT_PIECEWISE_LINEAR_PLASTICITY_TITLE

*PART

*SECTION_SHELL_TITLE

*MAT_RIGID_TITLE

*DEFINE_BOX

*DEFINE_CURVE_TITLE

*SET_NODE_LIST_TITLE

*CONSTRAINED_NODAL_RIGID_BODY

*ELEMENT_SHELL

*NODE

*END

Appendix G

Velocity curve plot values

(extracted from LS-PrePost® file)

Curveplot
LS-DYNA KEYWORD DECK BY LS-PREPOST
Time
Resultant Velocity
Node no.
100000 #pts=138
* Minval= 0.000000e+000 at time= 0.000000
* Maxval= 7.549602e+000 at time= 0.015998

0.000000e+000	0.000000e+000
9.993883e-004	4.030165e-001
1.998774e-003	1.048327e+000
2.998118e-003	1.690871e+000
3.997433e-003	2.378316e+000
4.999335e-003	3.078951e+000
5.998681e-003	3.731057e+000
6.998053e-003	4.333574e+000
7.997425e-003	4.835905e+000
8.999377e-003	5.278723e+000
9.998745e-003	5.666045e+000
1.099811e-002	6.017190e+000
1.199748e-002	6.337238e+000
1.299944e-002	6.651170e+000
1.399882e-002	6.952246e+000
1.499820e-002	7.257277e+000
1.599758e-002	7.549602e+000
1.699955e-002	7.467095e+000
1.799892e-002	7.268841e+000
1.899830e-002	7.089634e+000
1.999767e-002	6.781929e+000
2.099962e-002	6.486131e+000
2.199899e-002	6.257053e+000
2.299836e-002	5.958565e+000
2.399772e-002	5.623341e+000
2.499966e-002	5.400745e+000
2.599903e-002	5.161197e+000
2.699841e-002	4.889844e+000
2.799780e-002	4.677881e+000
2.899975e-002	4.533527e+000
2.999912e-002	4.331195e+000
3.099851e-002	4.185340e+000
3.199789e-002	4.004249e+000
3.299984e-002	3.854110e+000
3.399921e-002	3.656471e+000
3.499858e-002	3.448891e+000
3.599795e-002	3.366710e+000

3.699979e-002	3.250540e+000
3.799893e-002	3.073647e+000
3.899797e-002	2.953687e+000
3.999957e-002	2.917912e+000
4.099853e-002	2.888608e+000
4.199996e-002	2.869058e+000
4.299877e-002	2.776438e+000
4.399761e-002	2.637401e+000
4.499912e-002	2.532571e+000
4.599819e-002	2.540278e+000
4.699739e-002	2.578740e+000
4.799934e-002	2.622065e+000
4.899874e-002	2.475030e+000
4.999813e-002	2.315276e+000
5.099750e-002	2.174245e+000
5.199944e-002	2.013274e+000
5.299874e-002	1.947881e+000
5.399792e-002	1.759058e+000
5.499963e-002	1.678151e+000
5.599872e-002	1.774395e+000
5.699779e-002	1.775938e+000
5.799945e-002	1.832317e+000
5.899852e-002	1.977573e+000
5.999758e-002	2.340439e+000
6.099919e-002	2.771517e+000
6.199812e-002	3.101499e+000
6.299955e-002	3.350088e+000
6.399840e-002	3.254029e+000
6.499986e-002	3.208954e+000
6.599859e-002	3.029900e+000
6.699983e-002	2.697817e+000
6.799857e-002	2.345944e+000
6.899992e-002	2.144011e+000
6.999870e-002	1.804326e+000
7.099744e-002	1.550288e+000
7.199872e-002	1.280455e+000
7.299992e-002	1.054128e+000
7.399849e-002	7.354950e-001
7.499968e-002	6.728783e-001
7.599835e-002	6.090180e-001
7.699965e-002	5.668878e-001
7.799841e-002	5.228761e-001
7.899980e-002	5.553042e-001
7.999862e-002	7.581084e-001
8.099744e-002	1.026038e+000
8.199877e-002	1.206869e+000
8.299997e-002	1.164448e+000
8.399847e-002	1.098699e+000
8.499946e-002	1.056373e+000
8.599780e-002	1.223507e+000
8.699873e-002	1.481785e+000
8.799975e-002	1.638648e+000
8.899825e-002	1.649070e+000
8.999938e-002	1.709690e+000
9.099793e-002	1.789894e+000

```
    9.199905e-002    1.833423e+000
    9.299754e-002    1.959539e+000
    9.399861e-002    2.117664e+000
    9.499971e-002    2.222135e+000
    9.599818e-002    2.317610e+000
    9.699918e-002    2.405325e+000
    9.799760e-002    2.475123e+000
    9.899864e-002    2.506950e+000
    9.999976e-002    2.481283e+000
    1.009983e-001    2.411642e+000
    1.019995e-001    2.293884e+000
    1.029981e-001    2.230500e+000
    1.039992e-001    2.155568e+000
    1.049978e-001    2.097651e+000
    1.059989e-001    2.012108e+000
    1.069975e-001    1.934400e+000
    1.079986e-001    1.815334e+000
    1.089997e-001    1.787748e+000
    1.099983e-001    1.751232e+000
    1.109994e-001    1.733590e+000
    1.119979e-001    1.681682e+000
    1.129989e-001    1.615321e+000
    1.139999e-001    1.638336e+000
    1.149984e-001    1.702210e+000
    1.159994e-001    1.727791e+000
    1.169980e-001    1.657783e+000
    1.179991e-001    1.516445e+000
    1.189976e-001    1.256270e+000
    1.199987e-001    1.067778e+000
    1.209997e-001    9.019531e-001
    1.219982e-001    8.014492e-001
    1.229992e-001    7.803068e-001
    1.239975e-001    7.656010e-001
    1.249985e-001    8.325766e-001
    1.259995e-001    8.026766e-001
    1.269980e-001    6.391831e-001
    1.279992e-001    3.761985e-001
    1.289977e-001    6.401286e-002
    1.299989e-001    2.970446e-001
    1.310000e-001    6.264865e-001
    1.319986e-001    7.874596e-001
    1.329996e-001    6.595950e-001
    1.339981e-001    5.416376e-001
    1.349992e-001    5.345596e-001
    1.359977e-001    5.650653e-001
    1.368181e-001    6.276515e-001
endcurve
```

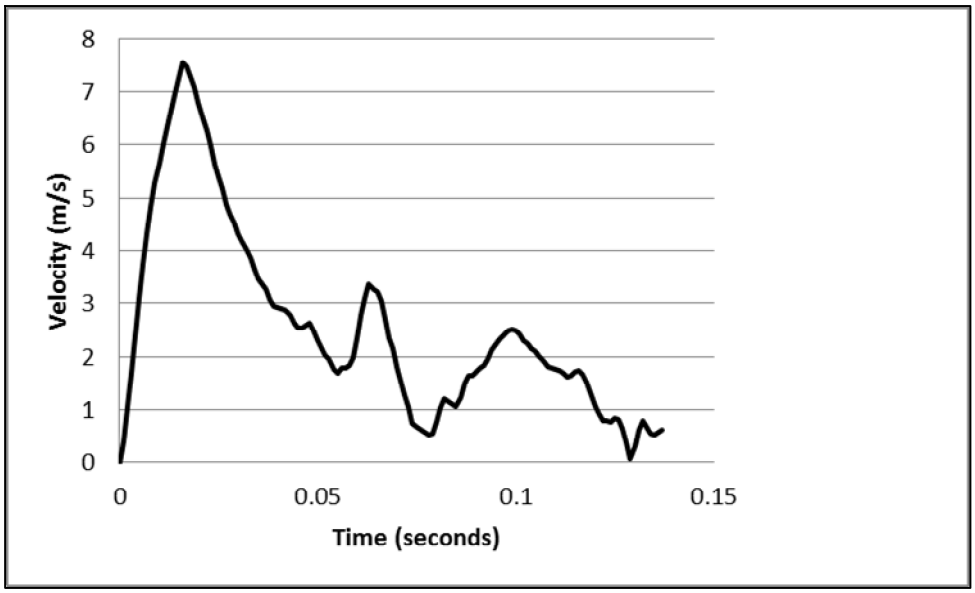

Figure F.1 - The LS-DYNA® velocity versus time